# Wave Group Forcing of Low Frequency Surf Zone Motion

by

**Robert P. Hamilton, Jr.**
**and**
**Robert A. Dalrymple**

RESEARCH REPORT NO. CACR-94-23
December, 1994

Center for Applied Coastal Research
Ocean Engineering Laboratory
University of Delaware
Newark, DE 19716

# TABLE OF CONTENTS

# LIST OF FIGURES

# LIST OF TABLES

# ABSTRACT

Wave group-induced radiation stresses are included in the nearshore hydrodynamic vorticity balance. It is shown how specific incident wave groups can provide the perturbations necessary for the generation of shear instabilities of the longshore current. Also, a resonant condition exists where low frequency, horizontal longshore current oscillations are initiated, and grow, from continual wave group forcing. These wave group forced current oscillations can continue after the forcing subsides due to the restoring force provided by the conservation of vorticity. Evidence of this phenomenon in nature is provided from the analysis of field data from the SUPERDUCK experiment, conducted in 1986. Spatially coherent wave groups are observed corresponding to times when strong low frequency surf zone motion exists. The incident wave climate has a bimodal direction-frequency wave spectrum, and high groupiness factors indicate significant wave groups. These groups are found to have periods and longshore spatial structure comparable to the low frequency surf zone motions, thus indicating the incident wave groups could have initiated the low frequency oscillations in the longshore current. A detailed laboratory experimental procedure is proposed to further identify and distinguish wave groups and instabilities in the longshore current as forcing mechanisms for low frequency surf zone motion.

# Chapter 1

# REVIEW OF LOW FREQUENCY SURF ZONE MOTION

Highly energetic low frequency fluid motions in the surf zone have recently been a topic of intense research interest because of their potential for inducing transport of beach sediments. Wind-generated waves are the fundamental source of this energy, and typically the shoreline is exposed to a complicated sea state consisting of numerous wave trains with different frequencies and incident directions. As these wave trains propagate onshore, shoal, and break, a significant amount of energy is transferred from higher wind wave frequencies to lower frequency motions due to the shallow water wave transformations. Other nearshore motions are forced by wave groups, resulting from the interaction of the different waves composing the sea state. In the surf zone, low frequency energy is manifested in the form of organized motions such as surf beat (Munk, 1949 and Tucker, 1950), edge waves (Lamb, 1932), migrating rip currents (Fowler and Dalrymple, 1990), meandering longshore currents (Ebersole and Dalrymple, 1979), and shear instabilities of the longshore current (Bowen and Holman, 1989). Wave groups have been demonstrated as a forcing mechanism for many of these phenomena, yet in the case of shear instabilities, the influence of the groups has not yet been established. Because of the high energy levels associated with these motions and the potential for significant sediment transport, a better understanding of their

dynamical properties and generation mechanisms is desired. Here, equations are formulated to explain how incident wave groups may force the current patterns attributed to shear waves, and an analysis of field data provides substance to the theoretical argument. Preceeding this discussion, an overview of the previously established low frequency surf zone motions and their forcing mechanisms is provided.

## 1.1 Surf Beat

First observed by Munk (1949) and Tucker (1950), surf beat has been defined as the long period, $O(10^3)$ sec, oscillations of the sea surface in the nearshore. These authors observed a correlation between the mean water level and wave groups. Longuet-Higgins and Stewart (1962) provided a physical explanation for these original observations with their discussion of radiation stresses. Essentially, as a group of high waves passes, there is a radiation stress that tends to force water from under the crest of the wave envelope, causing a depression of the sea surface, to the region under the trough of the envelope, where depth is locally increased. For successive incident wave groups, the mean water surface oscillation propagates in the direction of the swell at the speed of the wave group, with a ninety degree phase shift from the wave envelope. Gallagher (1971) later applied this physical argument, formulating a perturbation expansion of the wave equations where the surf beat arises as a second order solution forced by the non-linear interactions between the incident waves.

## 1.2 Edge Waves

Edge waves are well documented in the literature, with their dynamics being first discussed by Stokes (1846). Due to the refraction of gravity waves

on a sloping beach, there are waves trapped to the shoreline propagating in the alongshore direction. These trapped modes are edge waves, typically with large alongshore wavelengths and long periods. In the cross-shore direction, edge waves have an exponentially decaying oscillatory structure. Mathematically, an edge wave solution consists of the $n^{th}$ Laguerre polynomial, subject to the following dispersion relationship:

$$\omega^2 = g\, l\, (2n+1)\, m, \quad n = 0, 1, 2... \tag{1.1}$$

where $l$ is the longshore edge wavenumber and $m$ is the beach slope. The edge wave mode number, $n$, also indicates the number of zero crossings of the oscillatory cross-shore wave profile.

The generation mechanisms for edge waves vary, with a simple case being large angle incident waves reflecting from coastal structures and becoming trapped to the shoreline. Gallagher (1971) theoretically showed how incident wind waves and wave groups contribute to a second-order resonant response that can excite edge wave modes on the beach. A clearer physical understanding of this idea was obtained by Bowen and Guza (1978), who showed with a laboratory experiment that when the resonant conditions, discussed by Gallagher, are satisfied, edge waves are strongly active at the shoreline. Later, Huntley et al. (1981) provided strong evidence of edge wave modes in the field through analysis of the data collected at Torrey Pines Beach in 1978. Most recently, Nakamura and Katoh (1992) examined the relation between wave groups and infragravity waves by studying their cross-shore structure in field data, finding infragravity waves generated during the breaking processes of incident wave groups.

## 1.3 Migrating Rip Currents

Low frequency, meandering current patterns in the surf zone have been attributed to periodic rip current cells migrating along the shoreline. Dalrymple (1975) showed how two intersecting wave trains, incident from different angles with the same frequency, possess a wave group envelope forcing equally spaced circulation cells on the beach, due to the periodic reinforcement and cancellation of the incident wave field, resulting in a longshore variation in the radiation stress. Ebersole and Dalrymple (1979) observed when one wave train is larger, a longshore current is superimposed on the rip current field, giving a structured meandering longshore current pattern. This superposition argument is also supported by the following expression of the water surface for two incident linear wave trains:

$$\eta(\vec{x},t) = 2a_1 \sin\left(\frac{\Psi_1+\Psi_2}{2}\right)\cos\left(\frac{\Psi_1-\Psi_2}{2}\right) + (a_1-a_2)\sin\Psi_2, \qquad (1.2)$$

where $a_1$ and $a_2$ are wave amplitudes, and $\Psi_1$ and $\Psi_2$ are phase functions, represented by:

$$\Psi_i = \vec{k_i}\cdot\vec{x} - \omega_i t. \qquad (1.3)$$

In (1.3), $i = 1,2$, $\vec{k_i} = |k_i|\cos\theta_i\vec{i} + |k_i|\sin\theta_i\vec{j}$ is the wavenumber vector, where $(\vec{i},\vec{j})$ are the horizontal unit vectors in the $(x,y)$ directions, and $\omega_i$ is the angular frequency of the wave. Essentially, Equation (1.2) describes a modulated wave group that induces nearshore circulation cells, plus a plane wave train that adds a mean longshore current.

Later, Fowler and Dalrymple (1990) showed, in the laboratory, when the frequencies of these two wave trains are slightly different, the rip current cells migrate along the beach at a constant speed. Equations for predicting the spacing between the rip currents, $L_{gy}$, and the speed of propagation, $C_{gy}$, were derived as

follows:

$$L_{gy} = \frac{2\pi}{k_2 \sin\theta_2 - k_1 \sin\theta_1}, \text{ and} \tag{1.4}$$

$$C_{gy} = \frac{(\omega_1 - \omega_2)(k_1 \sin\theta_1 - k_2 \sin\theta_2)}{k_1^2 + k_2^2 - 2k_1 k_2 \cos(\theta_1 - \theta_2)}. \tag{1.5}$$

These theoretical predictions were shown to be fairly robust as laboratory measurements supported computations from (1.4) and (1.5) quite well. It is further expected that if one wave train is larger, a migrating meandering longshore current pattern would occur.

Tang and Dalrymple (1989) validated the existence of the migrating rip currents in the field using the same data as Huntley et al. (1981). Here, visual observations of this phenomenon were supported by spectral and statistical analyses, illustrating the offshore wave group structure correlated well with the surf zone motion. A canonical coherence analysis allowed for a determination of the maximum coherence between the offshore wave groups and the nearshore current motions, whose dominant structure was determined from a principal component (EOF) analysis. It was concluded that incident wave groups were a driving force for the nearshore circulation system at Torrey Pines Beach.

## 1.4 Shear Waves

Recently, Oltman-Shay et al. (1989) observed unique low frequency surf zone motions in the field data from the SUPERDUCK experiments, conducted at the U.S. Army Corps of Engineers Field Research Facility at Duck, North Carolina 1986. They noted horizontal oscillations in the longshore current propagating with a constant speed in the longshore direction, which occurred when the longshore current was strong. Based on these observations, Bowen and Holman (1989) formulated the shear wave theory, attributing the dynamic longshore current pattern

to a growing instability in the mean longshore current. The restoring force is a background vorticity supplied by the cross-shore profile of the longshore current. A simplified analytical solution was developed for a flat bottom and a bilinear cross-shore current profile, and the result was a prediction of currents similar to those observed in the SUPERDUCK data. Dodd et al. (1992) expanded the theory to include bottom dissipation, and Putrevu and Svendsen (1992) developed numerical solutions including the effects of more general bottom topographies, such as barred beaches.

Interestingly, in the shear wave problem formulation, the effect of the incident waves is solely to generate a longshore current, and wave group effects are neglected. Since it is known that incident waves and wave groups induce radiation stress variations dramatically affecting nearshore current dynamics, and wave groups are a significant forcing mechanism for other low frequency surf zone motions, their effect on the forcing of shear instabilities should be investigated as well. It is also intriguing that Dodd et al. (1992) studied the data from the NSTS field experiment at Leadbetter Beach, and concluded, depending upon the value of the friction coefficient, the observed low frequency surf zone motion could possibly be due to an instability in the mean longshore current. Yet, in the same study, they argue the surf zone motions may be directly attributed to long-time modulation of the incoming wave field, e.g., wave groups. Thus, motivation is provided for this present work, where wave group-induced radiation stresses are included in the momentum equations governing nearshore circulation patterns, and the shear wave theory, developed by Bowen and Holman (1989) is expanded to include these effects.

# Chapter 2

# THEORETICAL DEVELOPMENT OF WAVE GROUP FORCED LOW FREQUENCY MOTION

## 2.1 Governing Equation

The theoretical formulation parallels the shear wave theory developed by Bowen and Holman (1989), beginning with the shallow water, horizontal momentum equations:

$$\begin{aligned}
\frac{\partial u}{\partial t} + u\frac{\partial u}{\partial x} + v\frac{\partial u}{\partial y} &= -g\frac{\partial \eta}{\partial x} + \tau_x - \frac{\tau_{xz}^b}{\rho h}, \\
\frac{\partial v}{\partial t} + u\frac{\partial v}{\partial x} + v\frac{\partial v}{\partial y} &= -g\frac{\partial \eta}{\partial y} + \tau_y - \frac{\tau_{yz}^b}{\rho h},
\end{aligned} \tag{2.1}$$

where $u$ and $v$ are depth-averaged horizontal velocities, $\eta$ is the free surface displacement, and $g$ is the acceleration due to gravity. The total water depth, $h$, is a function of the cross-shore coordinate, $x$, and includes wave-induced set-down and set-up, so $h = d + \bar{\eta}$. Forcing due to wind stress, atmospheric pressure changes, turbulent shear stress, and Coriolis effects are neglected, while forcing due to hydrostatic pressure gradients, radiation stresses, and bottom dissipation through the bottom shear stresses ($\tau_{iz}^b$, $i = x, y$), are incorporated. Inclusion of the radiation stress, $(\tau_x, \tau_y)$, to the shear wave problem is unique to this formulation,

and permits the effects of incident waves and wave groups to be investigated. The radiation stress tensor in (2.1) has been abbreviated, similar to Bowen (1969), as:

$$\tau_x = -\frac{1}{\rho h}\left(\frac{\partial S_{xx}}{\partial x} + \frac{\partial S_{yx}}{\partial y}\right),$$
$$\tau_y = -\frac{1}{\rho h}\left(\frac{\partial S_{xy}}{\partial x} + \frac{\partial S_{yy}}{\partial y}\right). \tag{2.2}$$

Completing the equations of motion, the corresponding conservation of mass equation for an incompressible fluid under the rigid lid assumption is:

$$\frac{\partial (uh)}{\partial x} + \frac{\partial (vh)}{\partial y} = 0. \tag{2.3}$$

Given this set of governing equations, (2.1) and (2.3), the velocities in the surf zone are now assumed to be composed of a mean longshore current, $V(x)$, as a function of cross-shore position only, and small perturbations to the current, $u(x,y,t)$ and $v(x,y,t)$, varying in space and time. The total flow is expressed in vector form as:

$$\vec{u}_{tot} = \epsilon u(x,y,t)\hat{i} + [V(x) + \epsilon v(x,y,t)]\hat{j}, \tag{2.4}$$

where $\epsilon$ is a small number, and $\hat{i}$ and $\hat{j}$ are horizontal unit vectors. Similarly, the total water surface is assumed to be a superposition of short wind waves and small effects due to wave groups as follows:

$$\eta_{tot} = \eta_0(x,y,t) + \epsilon\eta_1(x,y,t), \tag{2.5}$$

where the subscript of 1 denotes wave groups. In turn, the corresponding short wave and wave group induced radiation stresses are distinguished as:

$$S_{xx} = S_{xx,0}(x,y) + \epsilon S_{xx,1}(x,y),$$
$$S_{xy} = S_{yx} = S_{xy,0}(x,y) + \epsilon S_{xy,1}(x,y),$$
$$S_{yy} = S_{yy,0}(x,y) + \epsilon S_{yy,1}(x,y). \tag{2.6}$$

Substituting expressions (2.4), (2.5), and (2.6) into (2.1), and linearizing with respect to the small parameter, $\epsilon$, allows for two distinct problems to be studied. The $O(\epsilon^0)$ problem governs the familiar cross-shore momentum balance determining wave set-up and set-down:

$$\frac{1}{\rho h}\left(\frac{\partial S_{xx,0}}{\partial x}+\frac{\partial S_{yx,0}}{\partial y}\right)=-g\frac{\partial \eta_0}{\partial x}, \tag{2.7}$$

while the $O(\epsilon^0)$ longshore momentum balance governs the generation of the longshore current:

$$\frac{1}{\rho h}\left(\frac{\partial S_{xy,0}}{\partial x}+\frac{\partial S_{yy,0}}{\partial y}\right)=-g\frac{\partial \eta_0}{\partial y}-\frac{\mu V}{h}. \tag{2.8}$$

The next problem, $O(\epsilon^1)$, is of particular interest here since it governs the dynamics of the deviations to the longshore current, $u$ and $v$, which are the source of low frequency surf zone oscillations. The $O(\epsilon^1)$ governing momentum equations are:

$$\begin{aligned}\frac{\partial u}{\partial t}+V\frac{\partial u}{\partial y}&=-g\frac{\partial \eta_1}{\partial x}+\tau_{x,1}-\frac{\mu u}{h},\\ \frac{\partial v}{\partial t}+u\frac{\partial V}{\partial x}+V\frac{\partial v}{\partial y}&=-g\frac{\partial \eta_1}{\partial y}+\tau_{y,1}-\frac{\mu v}{h}.\end{aligned} \tag{2.9}$$

Note in (2.7), (2.8), and (2.9), assumptions are made concerning the bottom dissipation. Following Dodd et al. (1992), the bottom dissipation is incorporated with linear dependence on the perturbation velocity, based on the discussion by Longuet-Higgins (1970), as follows:

$$\tau^b_{xz}=\epsilon\rho\mu u;\quad \tau^b_{yz}=\rho\mu V+\epsilon\rho\mu v, \tag{2.10}$$

where $\mu$ is:

$$\mu=\frac{2}{\pi}c_f U_o. \tag{2.11}$$

Here, $c_f$ is a dimensionless bottom friction coefficient, $U_o$ is the amplitude of the orbital swell velocity, and the $\frac{2}{\pi}$ factor comes from time averaging over the swell period. Inherent to the above formulation is the assumption, $U_o \gg V(x)$, which

will shown to be invalid for the SUPERDUCK data studied herein. However, Dodd et al. (1992) argue the assumption is applicable because only an order of magnitude estimation is required for the dissipative term.

Cross-differentiating and subtracting Equations (2.9) eliminates the dependence on $\eta$, the water surface. Based on the continuity Equation (2.3), a mass flux stream function, $\Psi$, may be defined as:

$$\begin{aligned} uh(x) &= -\frac{\partial \Psi}{\partial y}, \\ vh(x) &= \frac{\partial \Psi}{\partial x}. \end{aligned} \tag{2.12}$$

Substituting (2.12) in (2.9) for the perturbation velocities, $u$ and $v$, results in:

$$\begin{aligned} -\frac{\Psi_{yty}}{h} - \frac{V\Psi_{yyy}}{h} - \frac{\mu\Psi_{yy}}{h^2} - \frac{\partial \tau_{x,1}}{\partial y} &= \left(\frac{\Psi_{xt}}{h}\right)_x - \left(\frac{\Psi_y}{h}\right)_x V_x - \frac{\Psi_y}{h} V_{xx} \\ &+ V_x \frac{\Psi_{xy}}{h} + V\left(\frac{\Psi_{xy}}{h}\right)_x + \frac{\mu}{h}\left(\frac{\Psi_x}{h}\right)_x - \frac{\mu h_x \Psi_x}{h^3} - \frac{\partial \tau_{y,1}}{\partial x}, \end{aligned} \tag{2.13}$$

with all subscripts, except for those in the definitions for $\tau$, indicating partial derivatives. Further expansion of the derivatives and regrouping of the terms yields:

$$\begin{aligned} \left(\frac{\partial}{\partial t} + V\frac{\partial}{\partial y} + \frac{\mu}{h}\right)\left(-\frac{\Psi_{yy}}{h} - \frac{\Psi_{xx}}{h} + \frac{\Psi_x h_x}{h^2}\right) + \Psi_y \left(\frac{V_x}{h}\right)_x &= \\ -\frac{\mu h_x \Psi_x}{h^3} + \frac{\partial \tau_{x,1}}{\partial y} - \frac{\partial \tau_{y,1}}{\partial x}, \end{aligned} \tag{2.14}$$

where the left hand side, neglecting the bottom friction term, represents the conservation of potential vorticity, and the right hand side contains additional forcing terms due to bottom dissipation and wave groups. Neglecting the non-homogeneous forcing terms results in the eigensystem studied by Bowen and Holman (1989), who discovered the shear wave solutions by assuming the following form for the stream function:

$$\Psi = \mathbf{Re}\left\{\psi(x)\exp[i(k_y y - \sigma t)]\right\}, \tag{2.15}$$

with alongshore and temporal periodicity and unspecified cross-shore structure. Inherent to this assumption is a real alongshore wavenumber, $k_y$, and complex angular frequency, $\sigma$, and stream function. Under these assumptions, when the eigenvalue, $\sigma$, has a positive imaginary part, $\sigma = \sigma_{re} + i\sigma_{im}$, the solution for the wave of vorticity is unstable, growing exponentially in time:

$$\Psi = \exp(\sigma_{im}t)\mathbf{Re}\left\{\psi(x)\exp[i(k_y y - \sigma_{re}t)]\right\}. \tag{2.16}$$

The external forcing mechanisms are now included along with the following assumption about the periodicity of the wave group forcing:

$$\tau_{j,1} = \mathbf{Re}\left\{\tau_{j,1}(x)\exp[i(k_y y - \sigma t)]\right\}. \tag{2.17}$$

Substituting (2.17) and (2.15) into (2.14), the governing equation for the dynamics of externally forced waves of vorticity becomes:

$$\left(V - c_p - \frac{i\mu}{kh}\right)\left(\psi_{xx} - \psi k^2 - \frac{\psi_x h_x}{h}\right) - \psi h\left(\frac{V_x}{h}\right)_x = -\frac{i\mu h_x \psi_x}{kh^2} + \frac{ih}{k}\left(\frac{\partial \tau_{x,1}}{\partial y} - \frac{\partial \tau_{y,1}}{\partial x}\right), \tag{2.18}$$

where $c_p = \sigma/k$ is the celerity of the vorticity wave solutions.

Previous studies by Bowen and Holman (1989), Dodd et al. (1992), and Putrevu and Svendsen (1992) showed the homogeneous case of (2.18) is an eigensystem that admits real and complex eigenvalues for $\sigma$. For this case, the solutions with complex eigenvalues and positive imaginary parts are of greatest interest because of the resulting exponential temporal growth described by (2.16). These solutions for $\Psi$ are unstable horizontal velocity oscillations, occurring when an extremum in the potential vorticity profile, $V_x/h$, exists.

Most notable from the inhomogeneous Equation (2.18) is the possibility for wave group-forced solutions. Including the effects of the radiation stress gradients,

we discover two types of solutions to (2.18), suggesting interesting physical insight to the dynamics of longshore currents.

First, the unstable solutions of the homogeneous problem, shear waves, may be excited by randomness in the wave field or by incident short wave groups. These forcing mechanisms may initiate the perturbations in the background vorticity that grow temporally to a finite amplitude.

Second, there may be a resonant forcing of the stable solutions, with real $\sigma$, described by the inhomogeneous system. Since the addition of bottom dissipation to the homogeneous system inhibits a large number of the real eigenvalues, all but a few of the remaining stable solutions possess negative growth rates. This is especially important when wave group radiation stresses are incorporated, because a resonant response will be predicted corresponding to all real eigenvalues. Thus, incorporating bottom dissipation and wave group effects presents a governing system, forced by the wave groups with real $\sigma$ and $k$, and it is suspected (discussions with Uday Putrevu) that if the forcing frequency corresponds to an eigenvalue with a positive growth rate, a huge response may occur. In fact, resonant forcing of the solutions by the wave groups, with no exponential growth, can possibly create a current oscillation with an amplitude on par with the shear instabilities (discussions with Joan Oltman-Shay). Physically, this requires spatially structured, fairly stationary wave groups in the surf zone, existing long enough to resonantly force finite amplitude motion. Alternatively, if the wave group forcing corresponds to an eigenvalue with a negative growth rate, the response will be subdued. Interestingly, if the wave group forcing subsides, the homogeneous vorticity balance may provide a restoring mechanism, the background vorticity, maintaining the current oscillation without the presence of the wave groups. This may be a common physical scenario, since a wave climate is dynamic, and any

spatially coherent group structure may excite longshore current oscillations.

# Chapter 3

# DATA ANALYSIS TECHNIQUES AND THEORY

## 3.1 Pressure to Water Surface Conversion

The raw pressure signal, measured in the field from bottom mounted pressure gages, is detrended by subtracting the mean and a best fit second order polynomial, assumed to correspond to the pressure induced by the depth of the gage, and the tidal effects, respectively.

In order to study the incident wave climate, the detrended pressure data must be converted to a free surface displacement. This conversion is made via the pressure response factor from linear wave theory:

$$K_p(n) = \frac{\cosh[k(n)d]}{\cosh[k(n)h]}, \tag{3.1}$$

for each of the $n$ modes of the Fourier-transformed pressure time series, where $h$ is the water depth and $d$ is the distance from the gage to the bottom. The transfer function used to convert the Fourier modes of the pressure data, $F_p(n)$, to Fourier modes of a corresponding water surface, $F_\eta(n)$, is:

$$F_\eta(n) = \frac{1}{K_p(n)} F_p(n), \tag{3.2}$$

and an inverse Fourier transform may be applied to $F_\eta(n)$ to obtain a water surface time series.

Because of the constraints of linear wave theory, a number of assumptions are inherent to this conversion. First, the dispersion relationship, given by:

$$\omega(n)^2 = gk(n)\tanh(k(n)h), \tag{3.3}$$

allows for a wavenumber to be calculated corresponding to the angular frequency of each Fourier mode. Due to the depth attenuation of linear waves, high frequency motions should not be sensed by a gage mounted far below the water surface. For these high frequency wave motions, there is a very small pressure response factor (3.1), because $\cosh(kh) \gg \cosh(kd)$. Since the transfer function is inversely proportional to $K_p$, there will be an amplification of energy at these high frequencies. Thus, energy associated with frequencies corresponding to oscillations with a wavelength less than half the depth of the gage, the deep water cut-off, is filtered. This motion is attributed to instrument noise and pressure fluctuations due to bottom currents, and generally there is minimal energy loss associated with this truncation.

As a wave climate may be nonstationary, this conversion is computed for successive small chunks of the time series so the FFT analysis for waves at one time is not affected by different types of waves later in the data set.

### 3.2 Correlation Analysis

When analyzing the time series, it is often beneficial to compute the cross-correlation between various gages. In the results presented herein, the cross-correlation, as a function of time, between two time series, $x$ and $y$, with $N$ elements is defined as:

$$C_{xy}(m) = \frac{\sum_{n=0}^{N-|m|-1} x(n)y(n+m)}{C_{xy}(0)}, \tag{3.4}$$

which is normalized so a cross correlation at the zero time lag is unity.

### 3.3 Power Spectra

All power spectra are computed from a standard FFT analysis using the well known definition for the power spectral density function:

$$S(f) = 2\,|F_n|^2\,N\Delta t, \tag{3.5}$$

where $F_n$ is the Fourier transform of the time series, $N$ is the number of points in the time series, and $\Delta t$ is the data sampling rate. Spectral smoothing is accomplished by Bartlett averaging segments of data using a "box car" window, and spectral frequency band widths and statistical parameters are provided in the presented spectra.

### 3.4 Two-Dimensional Spectra

The development of reliable methods that can successfully estimate two-dimensional spectra from field data is crucial for this study. Specifically, direction and wavenumber versus frequency spectra provide key insight to the characteristics of the low frequency motions studied, and the credibility of the data analysis depends upon the reliability of the spectral analysis techniques. Following is a discussion of two methods that are developed, for determining the two-dimensional spectra. It is contended that comparable spectral estimates from two separate methods indicates accurate results. For a more detailed explanation of the methods used, and a users manual for the programs, the reader is referred to Hamilton and Dalrymple (1994).

#### 3.4.1 The Maximum Likelihood Method

The MLM was developed for the analysis of seismic waves by Capon et al. (1967), and first applied to the estimation of wavenumber spectra by Capon

(1969). Essentially, the MLM is a data adaptive procedure whereby the shape of the directional spreading function is determined from the data itself. It is assumed the data represents a clean wave train, termed the "true spectrum," plus additional noise. Davis and Regier (1977) explained the method completely and demonstrated its drawbacks and merits, finding that because the procedure is designed to extract a clean signal, it may not be best suited for certain data analyses. Expanding upon this point, Smith and Kaihatu (1989) showed, for a wave climate with broad directional spreading, the depiction of the directionality of the waves may develop multiple peaks. On the other hand, as confirmed by Pawka (1983), the method is clearly effective for resolving the directionality of distinct incident waves.

The theoretical development of the MLM is best explained by Isobe et al. (1982). To obtain the governing equation for the MLM directional spreading function, the aforementioned "true spectrum," weighted by a factor, is determined from the cross-spectra obtained from the Fourier transform of the time series from all the wave gage pairs. Next, a least-squared error problem is solved where the weighting factor is chosen so the response of the true spectrum to the noise is minimized. The equation used for computing the normalized directional spreading function in the MLM program is:

$$G(\theta,\omega) = \frac{\acute{\alpha}}{S(\omega)} \left\{ \sum_{ii=1}^{N} \sum_{j=1}^{N} (\Phi^{*}_{ii,j})^{-1} e^{ik(\omega) D_{ii,j} \cos(\theta - \beta_{ii,j})} \right\}^{-1}, \qquad (3.6)$$

where the variables are explained as follows:

$(\Phi^{*}_{ii,j})^{-1}$ = The inverse of the complex conjugate of the cross spectral matrix at each frequency for gages ii and j.

N = Number of gages.

$\acute{\alpha}$ = Normalization factor required to maintain an integral constraint

on the power. The total power must be consistently represented in $G(\theta, \omega)$ as it is in the power spectral density curve at each frequency.

$S(\omega)$ = The power spectral density value at each frequency.

$k(\omega)$ = Wavenumber.

$D_{ii,j}$ = Spatial lag between gages ii and j.

$\beta_{ii,j}$ = Angle between gages ii and j.

Equation (3.6) is generally useful for determining two-dimensional spreading functions, and is implemented with relatively easy programming and computational effort. The actual two-dimensional power spectrum is computed from the product of (3.6) with the value of the power spectral density function at each frequency. The independent variables in (3.6) are direction, $\theta$, and angular frequency, $\omega$, so an estimate of the direction-frequency spectrum can be obtained, provided the linear dispersion relationship, Equation (3.3), is assumed.

A variation to (3.6) is obtained by changing the exponential term as follows:

$$e^{ik(\omega)D_{ii,j}\cos(\theta-\beta_{ii,j})} \Rightarrow e^{ik_y D_{ii,j}}, \tag{3.7}$$

where the alongshore wavenumber, $k_y$, replaces $\theta$ as the second independent variable. In this case, an estimate of the wavenumber-frequency spectrum is obtained, which is particularly useful for analyzing the dynamics of periodic phenomenon not obeying (3.3). Note, in determining directional spectra, a two-dimensional gage array may be deployed, while only a linear shore-parallel array may be used for estimating alongshore wavenumber spectra. For details on the design of optimal gage array configurations, the reader is referred to Kirby (1993).

### 3.4.2 The Maximum Entropy Method

Initially, the Maximum Entropy Method (MEM) was only applied to the analysis of data from a pitch and roll buoy, or from a wave probe-current (p-u-v) meter. However, due to the widespread use of arrays of wave probes for measuring sea states, Nwogu (1989) developed a MEM approach for this case. The development of the theory begins with the simple expression for the cross-spectral density of the water surface, as a function of angular frequency, $\omega$, and incident wave angle, $\theta$, from two gages at different positions, $x_i$ and $x_j$, as follows:

$$S_{i,j}(\omega) = S(\omega) \int_{-\pi}^{\pi} \{i\vec{k} \cdot (\vec{x}_i - \vec{x}_j)\} \, D(\omega, \theta) d\theta. \tag{3.8}$$

Here, $S(\omega)$ is the power spectral density function and $D(\omega, \theta)$ is the angular spreading function, subject to an integral constraint of unity ($\int_{-\pi}^{\pi} D(\omega, \theta) d\theta = 1$), while wavenumber, $|\vec{k}|$, is related to frequency by the linear dispersion relation, (3.3). Equation (3.8) is re-expressed as a normalized cross-spectral matrix, $\Phi_j(\omega)$, in terms of an integral of the product of a matrix of kernel functions, $q_j(\theta)$, with the directional spreading function, $D(\omega, \theta)$ such that:

$$\Phi_j(\omega) = \int_{-\pi}^{\pi} q_j(\theta) D(\omega, \theta) d\theta. \tag{3.9}$$

Then, $D(\omega, \theta)$ is considered to be a probability of the direction of wave propagation as a function of the angle, $\theta$. By the definition from Shannon and Weaver (1949), entropy is now defined as:

$$E = -\int_{-\pi}^{\pi} D(\omega, \theta) \ln D(\omega, \theta) d\theta. \tag{3.10}$$

Maximizing (3.10), subject to the constraints imposed by the cross-spectral density matrix, is a variational problem yielding the following solution for $D(\omega, \theta)$:

$$D(\omega, \theta) = \exp\left\{-1 + \sum_{j=1}^{M+1} v_j q_j(\theta)\right\}, \tag{3.11}$$

in terms of the Lagrange multipliers, $v_j$. Substitution of the maximum entropy (3.11) into the cross-spectral matrix definition (3.9), results in a system of non-linear equations that can be solved, using orthonormal eigenvectors, and a Levenberg-Marquardt algorithm, for the unknown Lagrange multipliers in (3.11). Using (3.11), the solution for $D(\omega, \theta)$ can finally be obtained, and the direction-frequency spectrum can be computed from $S(\omega, \theta) = S(\omega)\, D(\omega, \theta)$, similar to the MLM. For more specific details on the MEM problem formulation and solution, the reader is referred to Nwogu (1989).

### 3.5 Phase Relationships from Cross-Spectra

The cross-spectral matrices used in estimating the two-dimensional spectra are also used for determining a number of phase characteristics. The cross-spectra of time series i and j is:

$$\begin{aligned} \Phi_{ij}(n) &= F_i^*(n) F_j(n) \\ &= |F_i(n)|\,|F_j(n)| \cos\left[\epsilon_i(n) - \epsilon_j(n)\right] \\ &\quad + i\,|F_i(n)|\,|F_j(n)| \sin\left[\epsilon_i(n) - \epsilon_j(n)\right], \end{aligned} \tag{3.12}$$

where the phase difference between gages $i$ and $j$ for frequency $n$ is represented by $[\epsilon_i(n) - \epsilon_j(n)]$. Therefore, the phase difference as a function of frequency may be calculated for any two gages as follows:

$$\Delta\epsilon_{i,j}(n) = \tan^{-1}\left(\frac{\mathbf{Re}\left\{\Phi_{ij}(n)\right\}}{\mathbf{Im}\left\{\Phi_{ij}(n)\right\}}\right). \tag{3.13}$$

Similarly, the phase difference as a function of spatial lag, at a specific frequency, for an array of gages may be computed from (3.13) by holding $n$ constant and varying the gages, $i$ and $j$. These operations are used extensively in the ensuing data analysis to provide valuable insight to the dynamics of periodic motions.

The last quantity calculated from the cross-spectra is the normalized squared coherence:

$$\gamma_{ij}^2(n) = \frac{|\Phi_{ij}(n)|^2}{\Phi_{ii}(n)\Phi_{jj}(n)}. \tag{3.14}$$

This quantity is useful for validating the pressure to water surface conversion, since a value of unity is expected for frequencies where the conversion is reliable.

### 3.6 Hilbert Transform

Because an analysis of the significance of wave groups and the wave group structure is required, the Hilbert Transform has been employed to obtain the wave envelope from the free surface data. This operation is defined as:

$$\zeta(t) = IFFT\left[F_\zeta = \begin{cases} F_\eta, & n = 0 \\ 2F_\eta, & 1 \leq n \leq N/2 - 1 \\ 0, & n \geq N/2 \end{cases}\right] \tag{3.15}$$

where the Fourier transform of the water surface, $F_\eta$, is used to obtain the transform of the wave envelope, $F_\zeta$, and $\zeta(t)$ is the wave envelope time series. For theory governing the Hilbert transform and similar causal functions, the reader is referred to Kirby (1993) or Bendat and Piersol (1986).

### 3.7 Wave Groupiness Factors

One measure of the significance of wave groups in water surface data is the groupiness factor, GF. First established by Funke and Mansard (1980), the GF was used to specify the importance of wave groups when generating waves in a laboratory flume. Fundamentally, the GF is defined as the standard deviation of the wave group envelope, or energy history, about its mean value. Larger GF values indicate more groupiness because the wave energy, propagating with the groups, has more peaks where sequential high waves exist in wave group crests.

Since the Hilbert transform was not yet established for the determination of the group envelope, the Smoothed Instantaneous Wave Energy History (SIWEH), developed by Funke and Mansard (1979), was utilized to represent the wave energy as a function of time. Computing the SIWEH, $E(t)$, requires a knowledge of a representative wave period for the data set, and this is chosen to be the spectral peak period, $T_p$. For each time step, an average square of the water surface displacement is computed from the surrounding data points spanning one representative wave period, as follows:

$$E(t) = \frac{1}{T_p} \int_{\tau=-T_p}^{T_p} \eta^2(t+\tau) Q(\tau) d\tau \quad T_p \leq t \leq T_n - T_p, \tag{3.16}$$

and for the ends of the time history:

$$\begin{aligned} E(t) &= \frac{2}{T_p + t} \int_{\tau=-t}^{T_p} \eta^2(t+\tau) Q(\tau) d\tau \qquad 0 \leq t \leq T_p, \\ E(t) &= \frac{2}{T_p + T_n - t} \int_{\tau=-T_p}^{T_n - t} \eta^2(t+\tau) Q(\tau) d\tau \quad T_n - T_p \leq t \leq T_n, \end{aligned} \tag{3.17}$$

where $T_n$ is the length of the time series. The SIWEH is smoothed using a triangular Bartlett window function, $Q(\tau)$, which modulates each computed average:

$$Q(\tau) = \begin{cases} 1 - \frac{|\tau|}{T_p} & -T_p \leq \tau \leq T_p \\ 0 & \text{all other } \tau. \end{cases} \tag{3.18}$$

Finally, the GF is computed from the SIWEH as follows:

$$GF = \left\{ \sqrt{\frac{1}{T_n} \int_0^{T_n} (E(t) - \bar{E})^2 \cdot dt} \right\} / \bar{E}, \tag{3.19}$$

where $\bar{E}$ is the mean of the SIWEH.

When computing the GF, it is also mandatory to filter motions corresponding to frequencies outside of the wind wave band from the time series. It is the intersection of wind waves that forms the wave groups, so low frequency energy contaminates the GF with bound waves that are phase-locked to the group structure, while high frequency motions may be due to instrumental noise. Mase (1990)

recommends filtering motions with a frequency less than one half the spectral peak frequency and motions greater than six times the peak frequency when computing the GF. In the case of bottom mounted sensors, high frequency oscillations above the deep water cutoff will contaminate the estimate of the GF, and should be filtered from the data.

# Chapter 4

# FIELD DATA OBSERVATIONS

The theoretical investigation of low frequency surf zone motions, described in Chapter 2, was inspired by the intriguing field observations of unique oscillating longshore currents made by Oltman-Shay et al. (1989). These authors examined cross-shore and longshore surf zone velocity records, and found remarkably coherent longshore current oscillations that propagated alongshore. Based solely on these observations, Bowen and Holman (1989) proposed the shear wave theory that explained some of the dynamics of these previously unobserved motions. Highly energetic surf zone motions of this type were observed corresponding to stormy sea conditions that generated strong alongshore currents. Thus, the objective of the following data analysis is to identify the extent to which the incident wave climate may have forced the observed surf zone motions. Particularly, the possibility of wave group-forcing of these motions, by initiation or resonance of the motion as described in Chapter 2, is investigated.

## 4.1 Overview of SUPERDUCK

The field data analyzed in this chapter was collected during the SUPERDUCK experiment conducted at the U.S. Army Corps of Engineers Field Research Facility (FRF) in Duck, North Carolina during September and October, 1986. The

goal of the experiment was to provide good quality data pertaining to nearshore phenomena, such as currents, waves, sediment transport, and bathymetry changes. Two specific days of data collection, October 10 and 15, 1986, were chosen for analysis based on the highly energetic low frequency motions observed by Oltman-Shay et al. (1989).

Velocity data was collected from an array of 10 Marsh-McBirney bi-directional current meters spanning 509 meters in the longshore direction. This array, illustrated in Figure 4.1, was situated about 50 meters seaward of the shoreline in the trough of a sandbar, and the minimum gage spacing was 10 meters. Each velocity meter was mounted at a depth of approximately 1 meter below mean sea level, and remained submerged at all times.

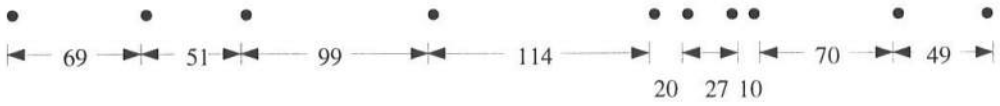


**Figure 4.1:** Bi-directional surf zone velocity meter array spacings (m) from the SUPERDUCK experiment, 1986.

Offshore pressure data was obtained from an array of 10 bottom-mounted pressure sensors, shown in Figure 4.2, spanning 254 meters in the longshore direction at a depth of about 8 meters. This depth corresponded to approximately 800 meters offshore, and was relatively deep water for the waves impinging during the experiment. Using the procedure discussed in Section 3.1, the incident wave climate can be estimated from this array.

Cross-shore pressure data was collected from a 7 gage array, and provided data for 92 meters extending from the velocity array in the surf zone to a position

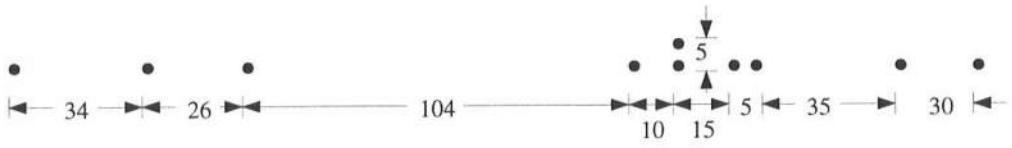


**Figure 4.2:** Pressure gage array spacings (m) from the SUPERDUCK experiment, 1986.

seaward of the sandbar. This data is most interesting for the analysis of the dynamics of incident waves and wave groups as they approach the surf zone and break.

Typically, data was collected in 4 hour intervals at 2 $Hz$. Contributions from tidal variations were minimized by centering each data sampling interval around a high or low tide. This way, the tidal variation was only about 0.2 meters during the data collection. The sampling rate allowed for waves and currents to be well resolved in time, while not making the data too voluminous.

## 4.2 Illustration of Surf Zone Motion

Figure 4.3 illustrates active meandering longshore currents from a sample of the longshore velocity data collected at SUPERDUCK. Notice the low frequency oscillation with period $O(10^2)$ seconds superimposed on wave motions with periods $O(10^1)$ seconds. Further, the mean of the signal indicates a strong mean longshore current of nearly 1.5 meters per second to the South.

Interestingly, for October 10, the "spin-up" of the low frequency current oscillation is observed. Figures 4.4 and 4.5 illustrate surf zone current velocity time series for the cross-shore and longshore velocities, respectively. The data

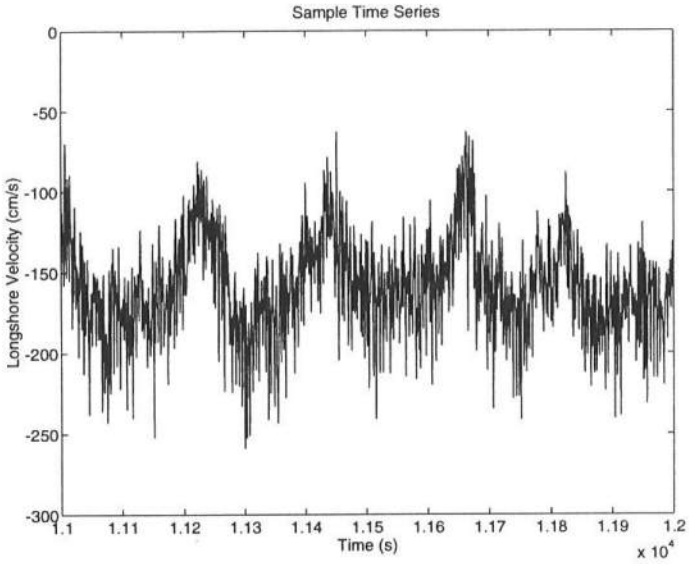


**Figure 4.3:** Time series section from gage LY06, SUPERDUCK, 10-10-86. 11,000 to 12,000 seconds of the data collection beginning at 04:00 AM.

has been low-pass filtered, neglecting motions above .01 $Hz$, to emphasize the very long period meandering longshore current. Approximately eight thousand seconds into the data collection, the long and cross-shore currents develop long period oscillations, with periods of about two hundred seconds. The amplitude of the current oscillation grows tremendously through the remaining time. Figure 4.5 also shows how the mean longshore current increases from approximately 0 meters per second to a strong 1.50 meters per second current flowing South. According to the field observations, this dynamic wave climate corresponds to the development of a local Nor'easter, which initiated highly energetic waves incident from the North.

In order to convey the coherent spatial structure of the meandering current, a normalized cross-correlation between the time series from various gages

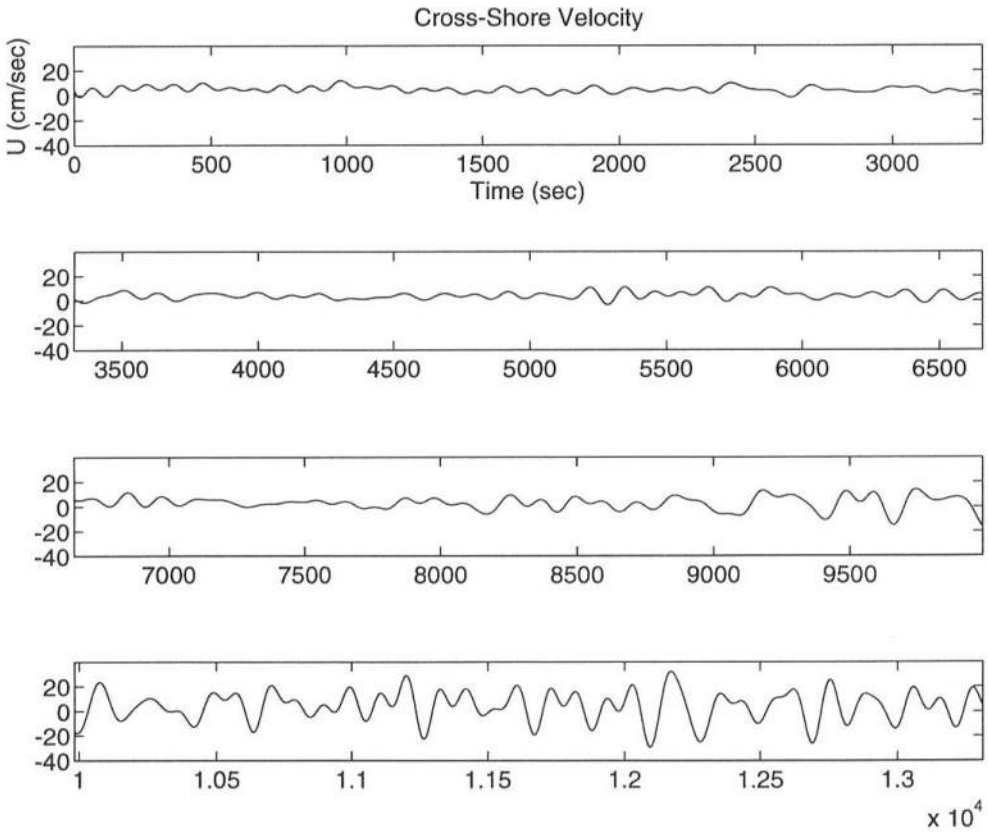


**Figure 4.4:** Fourier-filtered cross-shore velocity time series from gage LX07, SUPERDUCK, 10-10-86. 13,312 seconds spanning the entire collection period. Oscillations with frequencies above .01 $Hz$ are neglected.

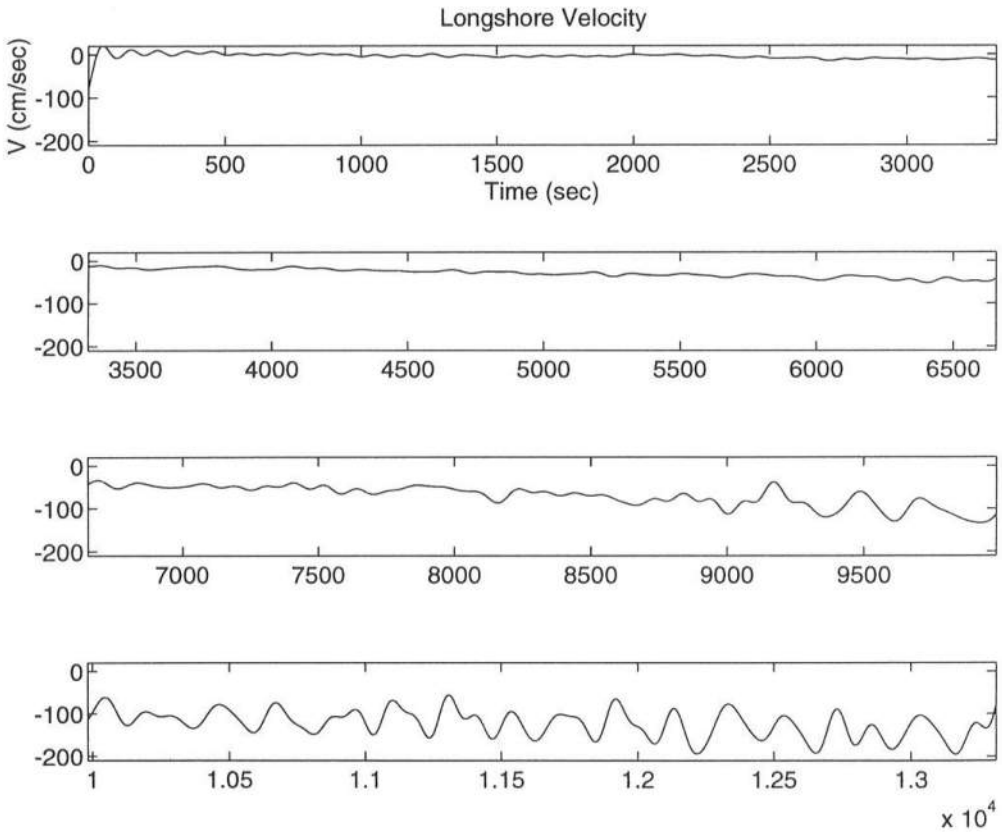


**Figure 4.5:** Fourier-filtered longshore velocity time series from gage LY07, SUPERDUCK, 10-10-86. 13,312 seconds spanning the entire collection period. Oscillations with frequencies above .01 $Hz$ are neglected.

is computed as described in Section 3.2. For example, Figure 4.6 illustrates the correlation of adjacent longshore velocity meters, LY01 and LY06 (176 meters apart in the surf zone), for the final 1024 seconds of data from October 10, when the shear waves (possibly wave group-forced) were active. The periodicity of the correlation and its high value, near 0.5, shows the current oscillation propagating in a coherent manner alongshore. A large negative correlation near a time lag of 80 seconds describes the dominant motions in the time series as exactly out of phase, while near 160, seconds the time series are in phase. Further, this indicates a phase speed of the dominant current oscillation to be $\frac{176m}{160s} \approx 1.1$ meters per second.

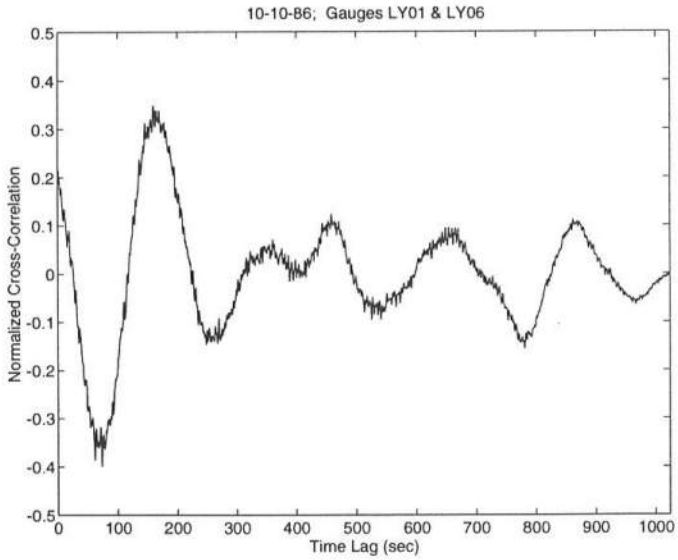


**Figure 4.6:** Normalized cross-correlation of longshore velocity meters, LY01 and LY06 spaced 176 m apart in the surf zone, for 10-10-86, SUPERDUCK. A value of one indicates perfect correlation.

The spatial structure of the current oscillation is illustrated in Figure 4.7, which is a plot of phase, at a frequency of $0.0029 Hz$, as a function of the longshore

spatial lag for all the meters measuring cross-shore velocity in the surf zone on October 15. Values of phase are obtained from all combinations of the cross-spectra between the velocity meters according to the discussion in Section 3.5. Essentially, a 360 degree change in phase represents a full wavelength of the meandering current motion at a chosen frequency. Here, the longshore periodic structure of the meandering current, with a frequency of 0.0029 $Hz$, is remarkably well illustrated for field data.

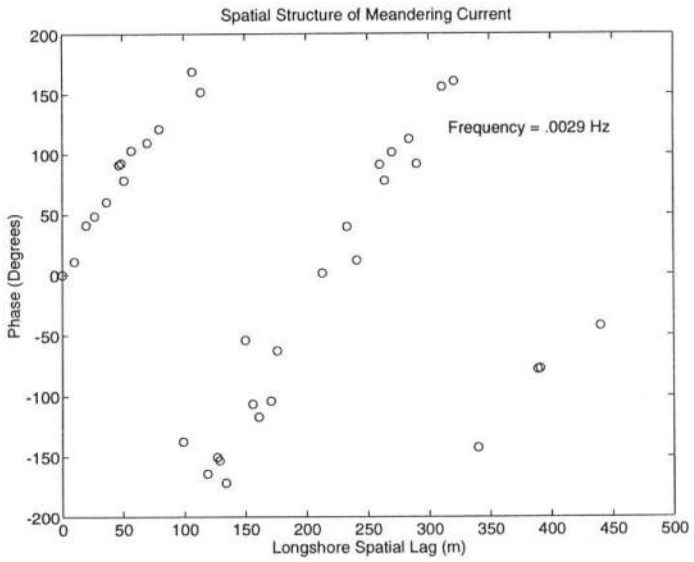


**Figure 4.7:** Phase versus longshore spatial lag for meters measuring cross-shore velocity in the surf zone, SUPERDUCK, 10-15-86. Gages LX01 - LX09, 26 D.O.F., $\Delta f = .001$.

Figures 4.8 and 4.9 illustrate the maximum likelihood estimate (MLE) of the magnitude of energy in the surf zone velocities as a function of frequency and cyclic longshore wavenumber ($1/L = k/(2\,\pi)$) for October 10 and 15, 1986. Of particular interest is the low frequency range, $0.0 - 0.01\ Hz$, where Oltman-Shay et al. (1989) noted a nearly linear relation between frequency and wavenumber. This implies a unique non-dispersive nature of the meandering current such that

the motion travels at a constant speed, independent of frequency. At higher frequencies, above 0.01 $Hz$, edge wave modes are shown to be strongly active in the surf zone as well.

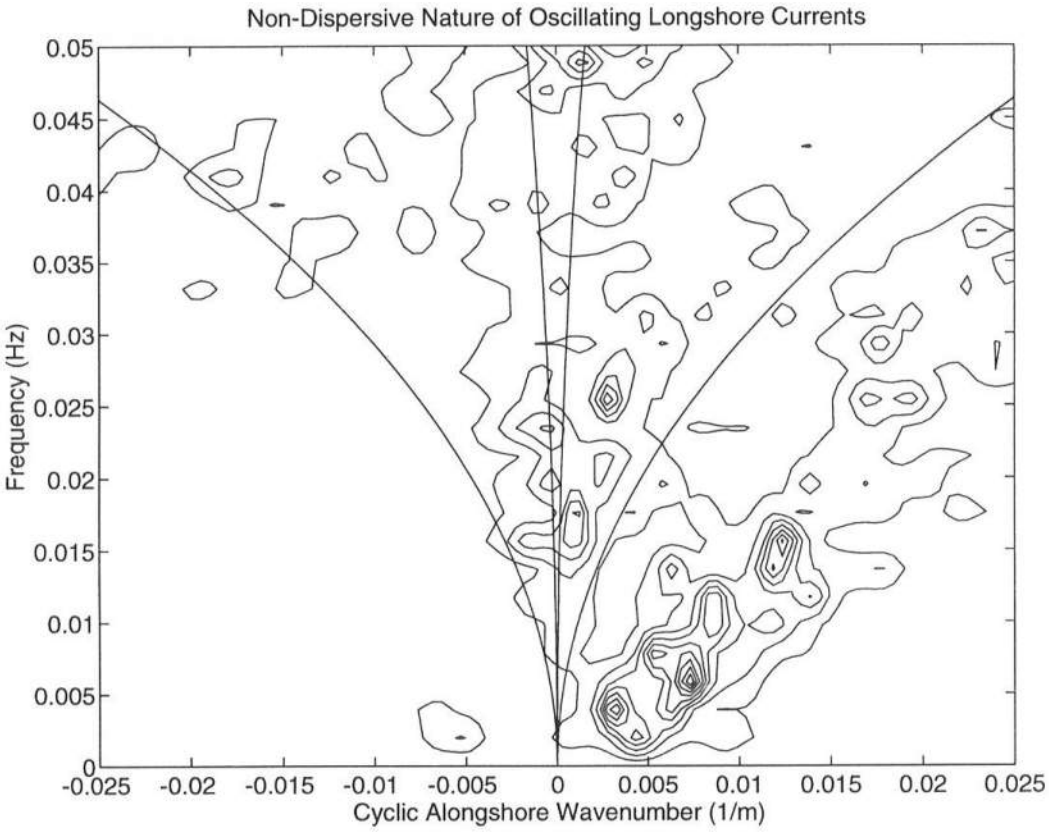


**Figure 4.8:** MLM estimate of the wavenumber-frequency normalized directional spreading function for cross-shore surf zone velocities for 10-10-86 for the final 85.33 minutes of data collection beginning @ 04:00 EST. Power is normalized for each frequency band, and contours represent tenths of peak power. Positive (negative) wavenumbers indicate southward (northward) propagation. 20 D.O.F., $\Delta f = .002$.

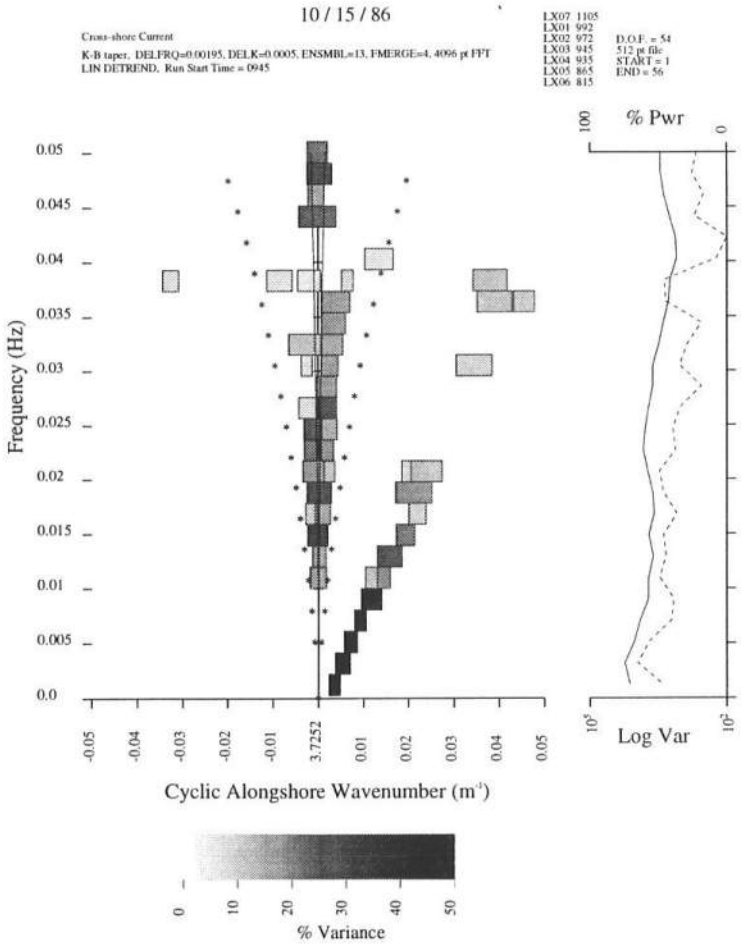


**Figure 4.9:** MLE wavenumber-frequency spectra of cross-shore surf zone velocities for 10-15-86 @09:45 EST. Positive (negative) wavenumbers indicate southward (northward) propagation. The rectangular boxes mark the location of variance peaks defined as those wavenumber maxima that have an adjacent valley below their half-power. The wavenumber width of each box is the half-power bandwidth of the peak. The shading density indicates the percent variance in the frequency bin that lies within the half-power bandwidth of the peak. Theoretical mode 0 edge wave dispersion curves for an effective plane beach slope of 0.055, and the leaky-trapped ($\sigma^2 = gk$) boundary are plotted. 54 D.O.F., $\Delta f = .002$. Obtained from Dr. Joan Oltman-Shay.

## 4.3 Demonstration of Wave Groupiness

Wave groups occur wherever the incident wave climate consists of wave trains with different frequencies and/or directions. The water surface is considered to be waves, traveling at the phase speed, modulated by an envelope traveling at the group velocity. The envelope is formed from the intersection of waves, perhaps incident from different directions, with different frequencies, and it describes the group spatial structure, which may be very complex when the sea state is broad banded in frequency as well as distributed in direction. In the following, the incident wave climate is estimated from offshore field wave data, corresponding to times when the low frequency motions are strongly active in the surf zone, and the waves are analyzed for group structure.

### 4.3.1 Water Surface Field Data

Using spectral analysis and the pressure response factor from small amplitude wave theory, a water surface displacement corresponding to the pressure data is computed as described in Section 3.1. A sample comparison between the pressure data and corresponding water surface is shown in 4.10. Recall from Section 3.1, there are high frequency pressure oscillations that should theoretically not be attributed to waves because of the depth attenuation of linear wave motion, and these have been neglected. To illustrate this effect, the squared coherence between pressure and water surface, computed according to Section 3.5, is illustrated in Figure 4.11. It is evident, due to a coherence of nearly unity, the water surface is accurate for frequencies ranging from 0.0 $Hz$ through the highest expected wind wave frequencies, but the coherence is near zero for high frequency motions past the deepwater cut-off.

The possibility of a nonstationary wave climate is permitted by making the pressure to water surface conversion for thirteen blocks of data, spanning the time series. This is particularly important for the October 10 wave climate, which is nonstationary, and the waves at the end of the data collection should have no influence on the FFT analysis of the waves in the beginning of data collection.

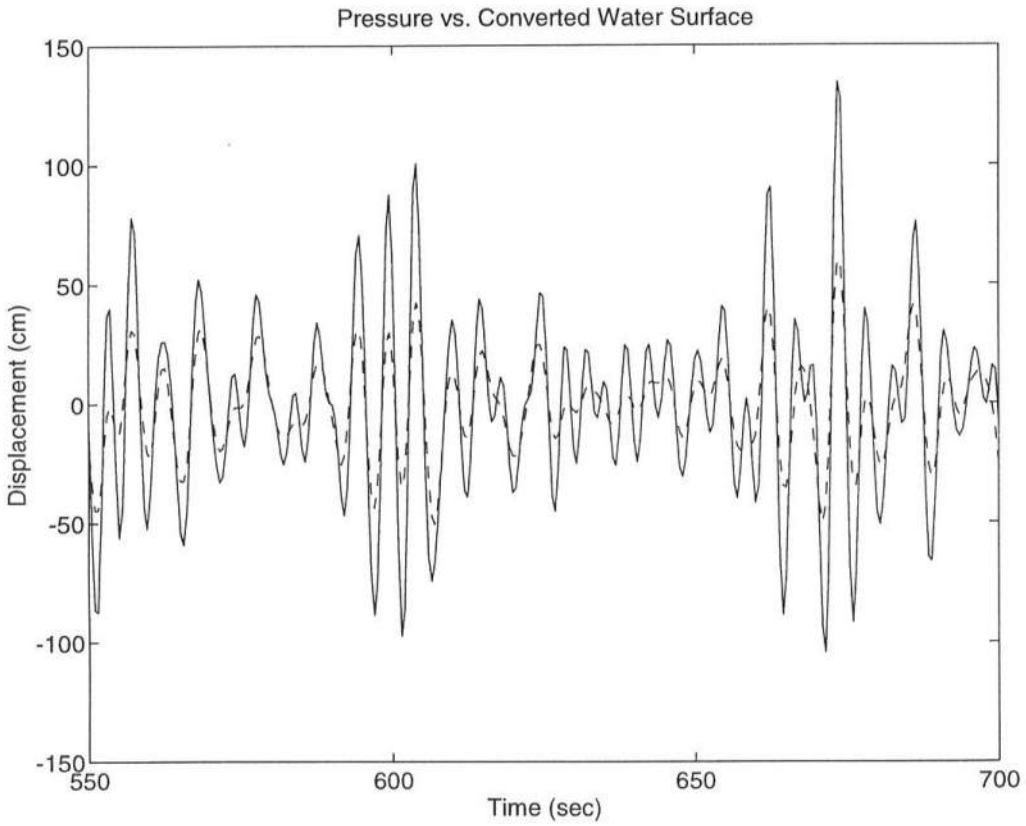


**Figure 4.10:** Comparison of detrended raw pressure data (dotted line) and the corresponding water surface from linear theory (solid line). Gage LA05 from SUPERDUCK, 10-15-86.

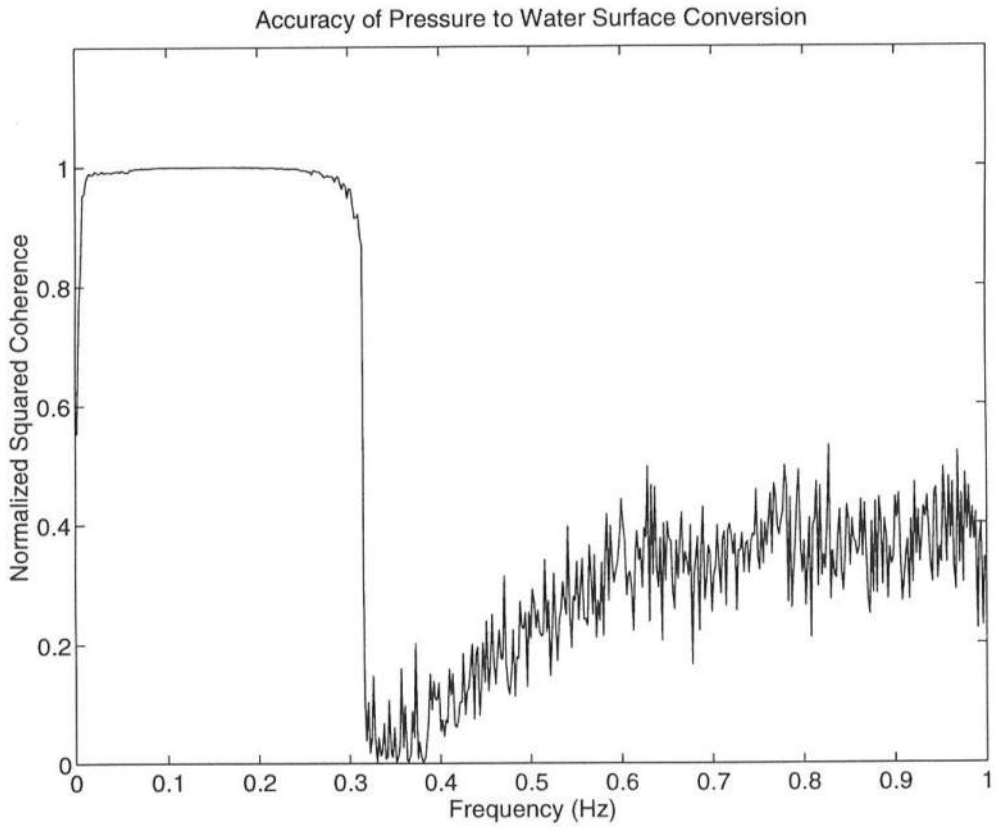


**Figure 4.11:** Normalized squared coherence between detrended pressure and converted water surface data. Gage LA05 from SUPERDUCK, 10-15-86.

### 4.3.2 The Incident Wave Climate

The wave climate is analyzed for October 10 and October 15, 1986 at 04:00 and 09:45 EST, respectively, corresponding to times of strong low frequency surf zone motion. The two-dimensional frequency and direction wave spectra of the incident wave climate are obtained using the Maximum Likelihood Method (MLM, described in Section 3.4.1) and the Maximum Entropy Method (MEM, described in Section 3.4.2), provided by Nwogu (1989). Two methods are used in order to improve the confidence in the depiction of the water surface, and it is found the MLM and MEM result in very nearly the same representation of the water surface for the data studied.

#### 4.3.2.1 Testing for Stationarity in the Wave Climate

Prior to the computation of reliable estimates for the two-dimensional spectra, time-varying characteristics of the data must be investigated. The Bartlett averaged cross-spectra used in the MLM and MEM computations only provide a realistic result if the data depicts a stationary process. Otherwise, the resulting spectra describe an average wave climate over the data collection period, but at any given time the actual incident waves may be dramatically different.

Recalling the time-varying surf zone currents depicted in Figures 4.4 and 4.5, the wave climate for the October 10 data collection period is expected to have temporal variations as well. Insight to the dynamic wave climate is gained by dividing the near four hours of data into three segments of approximately one hour (68.27 minutes) each. Specifically, bins of 8192 points are analyzed using short Bartlett blocks of 512 points, retaining a statistically reliable spectral estimate with 32 degrees of freedom.

Figure 4.12 illustrates a dramatic change in the power spectra as the winds from the storm generated increasing wave energy. Typical for stormy conditions, high energy, short wind waves were formed near 0.3 $Hz$, and as time progressed the effects of frequency dispersion reduced the spectral peak frequency to nearly 0.2 $Hz$. The reduction of the spectral peak frequency is an indication that a fairly stationary stormy sea state may have developed toward the end of the data collection period. This is confirmed by further subdividing the data toward the end of the record, for which the power spectrum is less dynamic.

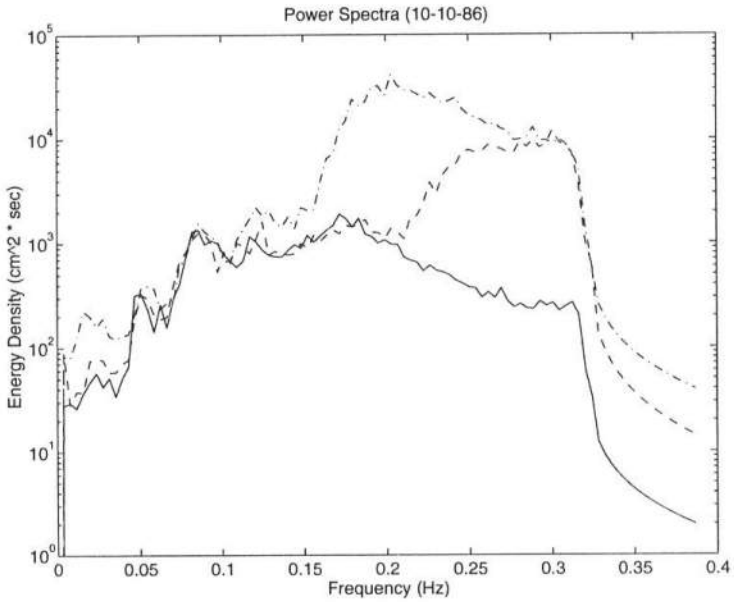


**Figure 4.12:** Comparison of water surface power spectra for SUPERDUCK, 10-10-86. First 68.27 minutes (——), second 68.27 minutes (- - -), and third 68.27 minutes (-·-·-·). 32 D.O.F., $\Delta f = 0.0039\ Hz$.

Having identified temporal variations in the power spectra for October 10, MLM direction-frequency spectral estimates for the three blocks of data are presented in Figures 4.13, 4.14, and 4.15. Figure 4.13 depicts the pre-storm sea state as a low energy background swell from the South, with predominant energy

incident from $-50^o$ from the beach normal, and spanning a frequency range of $0.1-0.2\,Hz$. As the storm developed, Figure 4.14 illustrates the evolution of short wind waves with frequencies of $0.25-0.30\,Hz$, with broad directional spreading around an incident angle of $40^o$ from the North. Once the storm is established, Figure 4.15 describes a sea state with dominant energy incident from an angle of about $40^o$ counterclockwise from the beach normal, and with frequency spreading centered around $0.20\ Hz$. The oblique incident wave angle associated with these wind waves is also consistent the time series in Figures 4.3, 4.4, and 4.5, as the energetic wind waves associated with the Nor'easter forced the strong South directed mean longshore current. The source of the oscillating current motion is addressed in the forthcoming sections.

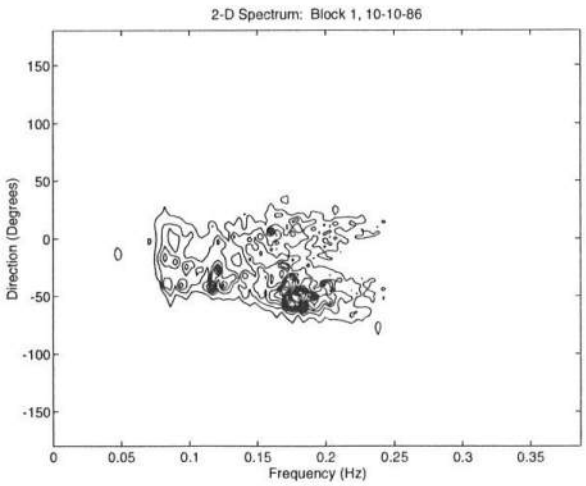


**Figure 4.13:** MLM estimate of the two-dimensional direction and frequency wave spectrum for the first 68.27 minutes of SUPERDUCK, 10-10-86 @ 04:00 EST. Contours are tenths of maximum power. 32 D.O.F., $\Delta f = 0.0039\ Hz$.

The stationarity of the October 15 wave climate is confirmed by simply comparing the incident wave power spectra. Figure 4.16 shows for three segments of the data, the power spectra is virtually unchanged, and the wave climate

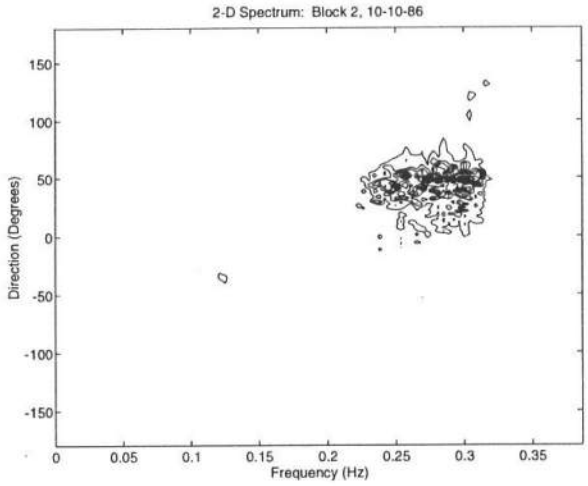


**Figure 4.14:** MLM estimate of the two-dimensional direction and frequency wave spectrum for the second 68.27 minutes of SUPERDUCK, 10-10-86 @ 04:00 EST. Contours are tenths of maximum power. 32 D.O.F., $\Delta f = 0.0039\ Hz$.

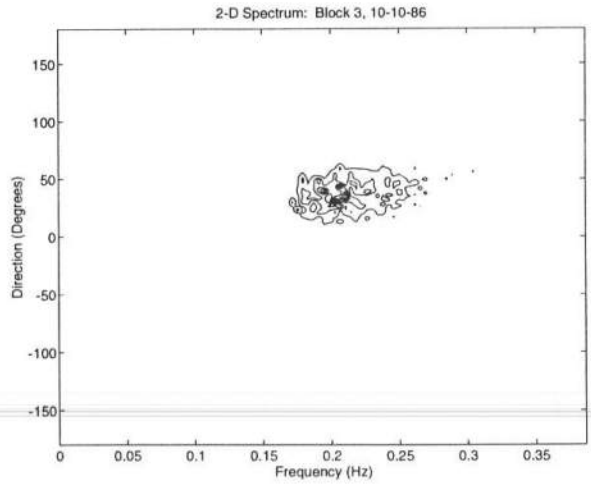


**Figure 4.15:** MLM estimate of the two-dimensional direction and frequency wave spectrum for the third 68.27 minutes of SUPERDUCK, 10-10-86 @ 04:00 EST. Contours are tenths of maximum power. 32 D.O.F., $\Delta f = 0.0039\ Hz$.

is stationary. Further analysis of temporal variations of the direction-frequency spectrum for this data set, similar to Figures 4.13 to 4.15, describe a stationary wave climate as well.

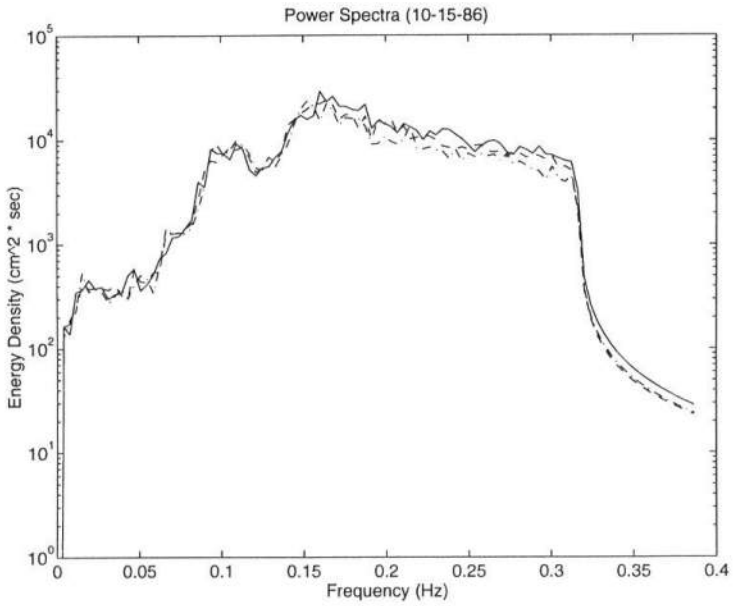


**Figure 4.16:** Comparison of water surface power spectra for SUPERDUCK, 10-15-86. First 68.27 minutes (——), second 68.27 minutes (- - -), and third 68.27 minutes (·····). 32 D.O.F., $\Delta f = 0.0039\ Hz$.

#### 4.3.2.2 Presentation of Two-Dimensional Wave Spectra

In consideration of stationarity, the third time block of the October $10^{th}$ time series used to generate Figure 4.15, plus the remaining 17 minutes, is adopted for the MLM direction-frequency spectrum. Figure 4.17 is a surface plot and perspective contours of the direction-frequency spectra for this data. For October 15, Figure 4.19 represents the MLM estimated spectrum that is averaged over the entire collection period, due to the stationarity of the data. Similar to the wave climate for October 10, there is a dominant source of wind wave energy.

Arguably, the MLM does not provide the best estimate of directional wave spectra for broad banded sea states, because the method is designed to extract plane wave signals from the data. Therefore, to validate the estimates of the directional sea state, the MEM is employed as well. The results from the MEM are illustrated in Figures 4.18 and 4.20, and the similarity of these plots to Figures 4.17 and 4.19, for the MLM, confirm the sea state is well represented. The MEM estimated spectra for October 10 is for the third block of data, which is expected to describe a fairly stationary storm sea state.

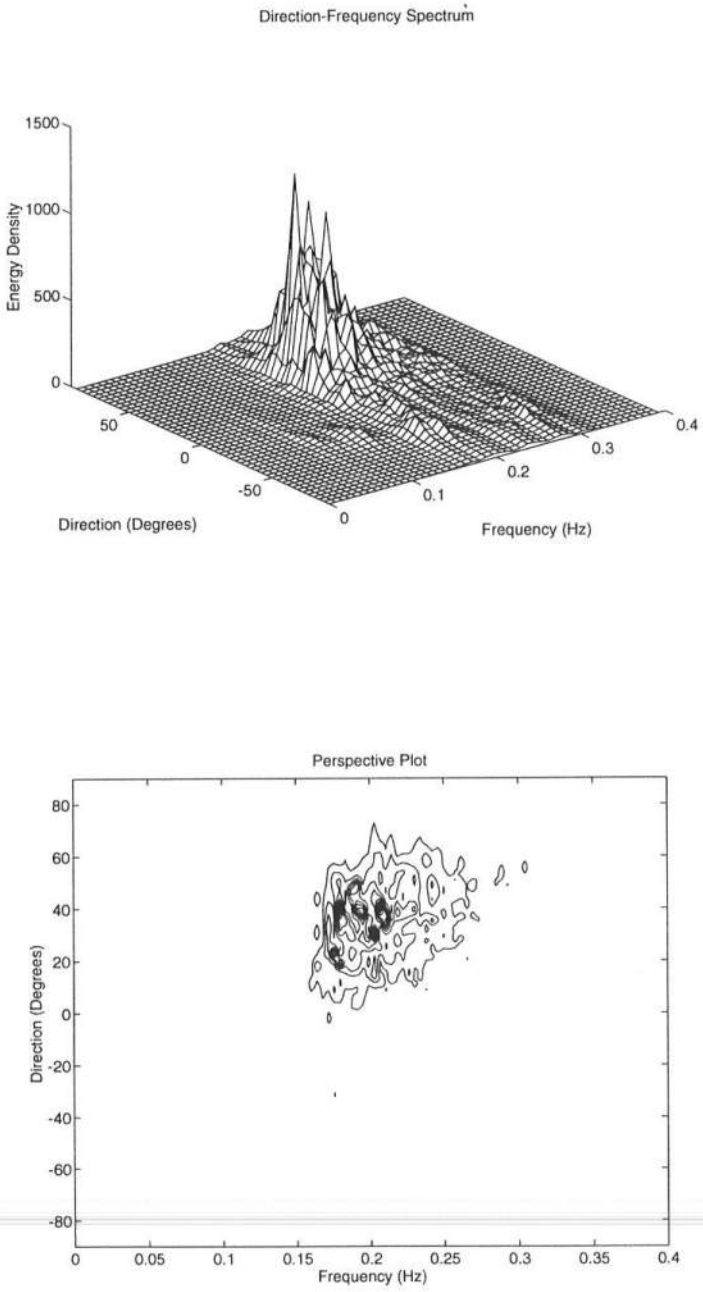


**Figure 4.17:** MLM estimated two-dimensional wave spectrum from SUPER-DUCK, 10-10-86 for the final 85.33 minutes. Using all offshore pressure sensors, LA01-LA10. Contours represent tenths of peak power. 40 D.O.F., $\Delta f = .0039$.

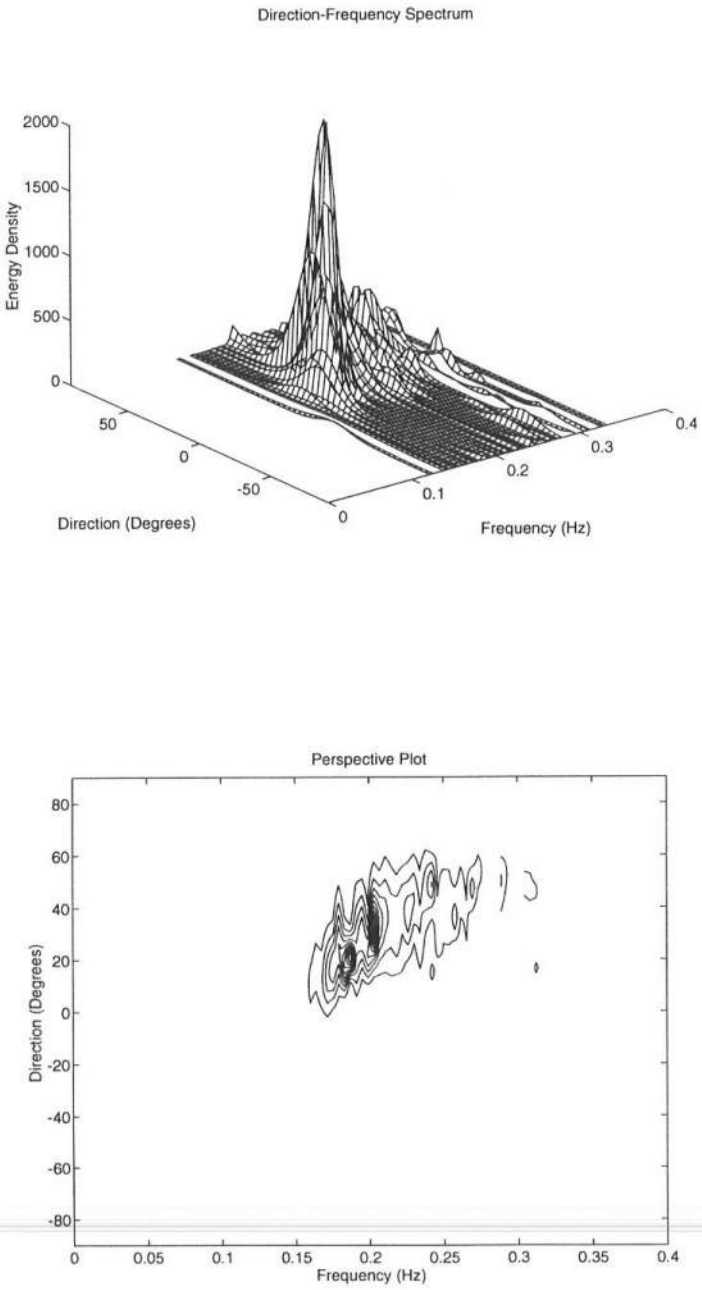


**Figure 4.18:** MEM estimated two-dimensional wave spectrum from SUPER-DUCK, 10-10-86 for the final 85.33 minutes. Using the following offshore pressure sensors: LA01-LA04 and LA10. Contours represent tenths of peak power. 40 D.O.F., $\Delta f = .0039$.

Of particular interest in this present work is the frequency and directional spreading of energy depicted in Figures 4.17 through 4.20, which forms a wave group envelope that modulates the water surface. Here, the most energetic waves, surrounding 0.2 $Hz$ at 35 degrees, and 0.16 $Hz$ at 30 degrees for October 10 and 15, respectively, have a localized spreading of energy that is expected to form a significant wave group structure.

In addition to the local spreading of energy, there is also evidence of a bimodal wave climate. For example, Figures 4.19 and 4.20 illustrate, in addition to the locally generated wind waves, there are waves representative of a background swell with a frequency of 0.1 $Hz$ incident from an opposite direction. This is a unique sea state, because the locally generated waves could have the same incident angle as the low frequency swell. In that case, as time progressed and the locally generated wind waves formed lower frequencies, the two groupings of energy would be indistinguishable. However, for the two sets of data depicted in Figures 4.17 through 4.20, the frequencies and directions are distinct.

Examination of Figures 4.13 to 4.15 reveals a bimodal wave climate for October 10 as well, with a similar swell incident from the South that is much less energetic than the locally generated storm waves. Based on Equation (1.2) of Fowler and Dalrymple (1990), the intersection of these waves results in a wave group modulated water surface plus an additional obliquely incident wave train, and may induce meandering migrating rip currents in the nearshore.

Reviewing Figures 4.4 and 4.5, a wave group-induced surf zone current pattern is potentially implicated for October 10. Approximately eight thousand seconds into the data collection, the storm wave energy may be equal to the energy of the background swell (it is not possible to distinguish exactly when the storm wave energy matched the energy of the background swell because of the

need for an accurate spectral analysis of a nonstationary process), and migrating rip currents were induced in the surf zone. Beyond this time, the additional storm wave energy increased the velocity of the longshore current. When superimposed on the existing rip current field, it may have resulted in a migrating, meandering longshore current, which is very similar to the motion predicted by the shear wave theory. It is also possible that incident wave groups provided the perturbation necessary to initiate the shear instability to the longshore current, and that continual wave group forcing may have resonated the current oscillation, causing faster growth to a larger amplitude. While merely a conjecture, because a detailed time varying incident wave climate cannot be sucessfully analyzed, this is evidence for the significance of wave groups in forming low frequency current oscillations. In the following, these wave groups will be identified.

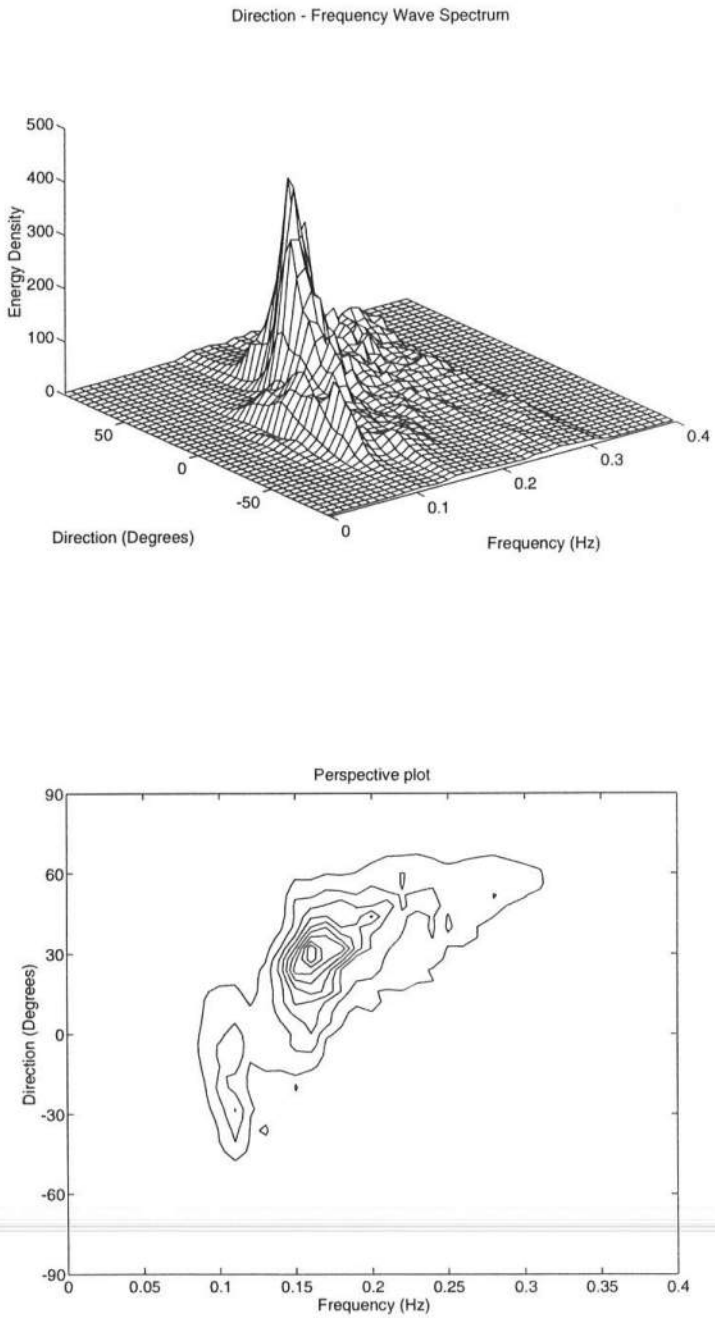


**Figure 4.19:** MLM estimated two-dimensional wave spectrum, SUPERDUCK, 10-15-86. Using all offshore pressure sensors, LA01-LA09. Contours represent tenths of peak power. 52 D.O.F., $\Delta f = .002$.

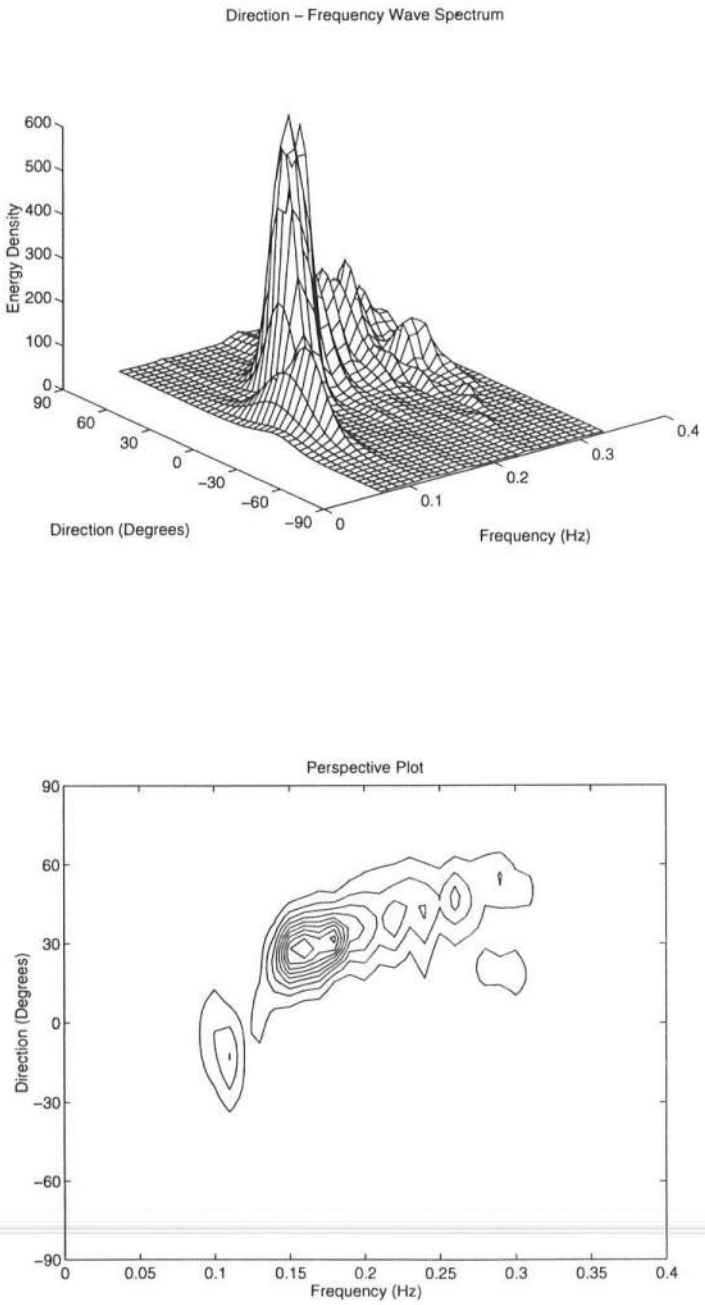


**Figure 4.20:** MEM estimated two-dimensional wave spectrum, SUPERDUCK, 10-15-86. Using the following offshore pressure sensors: LA01-LA04. Contours represent tenths of peak power. 52 D.O.F., $\Delta f = .002$.

### 4.3.3 Significance of Wave Groups in the Data

Wave groups are detected and analyzed by calculating the groupiness factor, GF, and by computing the Hilbert transform of the water surface data as described by Bendat and Piersol (1986). The Hilbert transform of a wave train signal gives the variation of the wave envelope as a continuous function of space and time.

The GF is computed as defined in Section 3.7, and in this case, $T_n$ is chosen such that the GF could be averaged over the data set with 52 degrees of freedom. Funke and Mansard (1980) studied six months of field data from the Sea of Japan and found a typical range to be: $0.46 \leq GF \leq 0.94$. Similarly, Yu and Liu (1990) studied 73 field records from Shiyiu Port, China and found the typical range to be: $0.36 \leq GF \leq 0.93$. These ranges are for offshore wave data. Other work by Mase et al. (1990) has shown the GF decreases rapidly as waves break across the surf zone.

When calculating the GF for the SUPERDUCK data, a standard procedure suggested by Mase et al. (1990) is used to focus on the wave groups formed by wind generated waves. Fourier filtering is used so all modes relating to frequencies less than half the peak or greater than six times the peak frequency are set equal to zero. This is especially important for the gages in the surf zone where waves are broken and energy has been transferred to other low frequency motions not related to wind wave groups. The GF has been computed for the offshore waves as well as from the cross-shore data, and the values are listed in Table 4.1.

Based on the table and the previously discussed range of typical GF values, it is evident there are significant wave groups in the SUPERDUCK data. For example, the GF values from the sensor furthest offshore are above 0.75 for both

**Table 4.1:** Groupiness Factor as a function of cross-shore distance. Significant wave breaking occurred at approximately 200 meters.

| Cross-Shore Coordinate (m) | Groupiness Factor | |
|---|---|---|
| | 10-10 | 10-15 |
| 914 | 0.7815 | 0.7554 |
| 217 | 0.7136 | 0.5638 |
| 200 | 0.6454 | 0.5950 |
| 187 | 0.5773 | 0.6023 |
| 178 | 0.7090 | 0.5524 |
| 169 | 0.5513 | 0.6065 |
| 155 | 0.5322 | 0.6125 |

days and this indicates strong incident wave group structure. Noting that waves break on the sand bar, approximately 200 meters offshore, even the GF values in the surf zone have values near 0.6, indicating moderate wave groupiness. The consistently groupy structure through the surf zone provides a strong indication that analysis of the offshore wave groups will be insightful for determining their role in forcing surf zone motions. However, it is not even required that the group structure exist in the surf zone. This is because shear wave motions extend offshore beyond the breaker zone where randomness in the wave field or a spatially coherent wave group may provide the perturbations or resonant forcing for the horizontal longshore current oscillations.

The wave envelope is studied by taking the absolute value of the Hilbert transform (defined in Section 3.6). Figure 4.21 demonstrates the effectiveness of this method in obtaining the wave envelope for a portion of the data from an offshore sensor. The mirror image of the envelope has been plotted as well to effectively illustrate the groups. Higher frequency oscillations in the envelope, above 0.033 $Hz$, are filtered by equating the corresponding Fourier coefficients

with zero. It is visually obvious from Figure 4.21 that the expectation of wave groups due to the frequency and directional spreading of energy, the bimodal sea, and the high GF is justified.

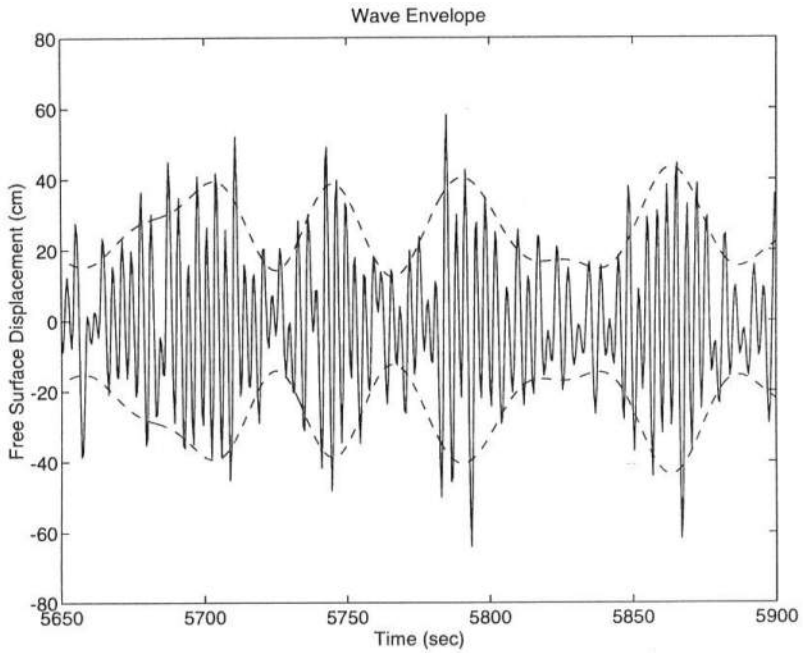


**Figure 4.21:** Wave data and filtered group envelope, from the absolute value of the Hilbert transform, for offshore pressure sensor LA01. Portion of the time series for data collection beginning at 04:00 EST, 10-10-86.

### 4.3.4 Wave Group Structure and Forcing of Surf Zone Motions

The power spectra of the wave envelope time series, computed from the Hilbert transform, is compared to the spectrum of the free surface in Figure 4.22 for the two days of interest. Especially noteworthy is the large amount of power contained in the wave groups for low frequency motions ranging from 0.0 to $0.1\,Hz$. This suggests powerful wave groups at a range of frequencies spanning the

far-infragravity (FIG) and infragravity frequency bands where shear instabilities, propagating meandering currents, migrating rip currents, and edge wave motions occur.

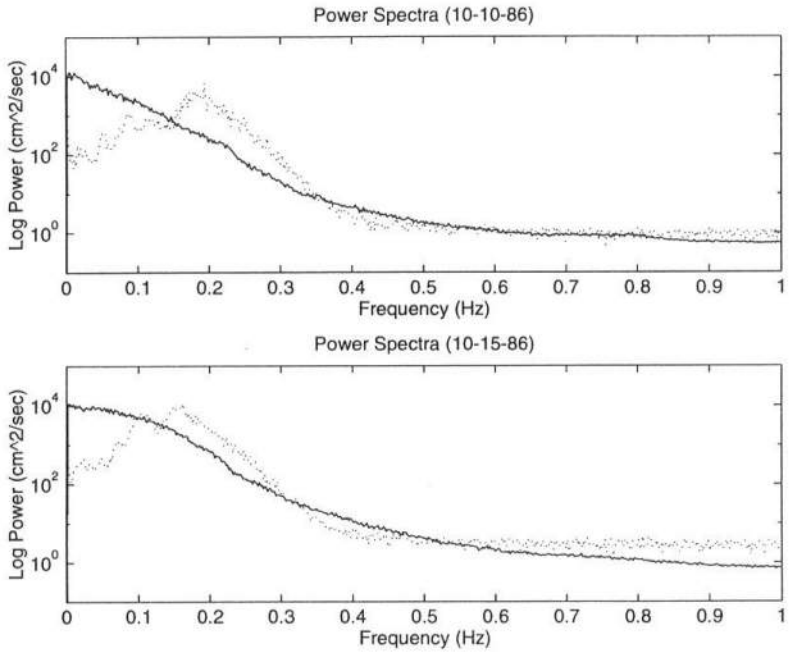


**Figure 4.22:** Power spectra for waves (dotted) and wave groups (solid). 52 D.O.F., $\Delta f = .002$. Group spectra are an average of the Hilbert transformed free surface signal from all the offshore gages. Wave spectra are from the pressure record from gage LA09.

Additional information is available by using the MLM to determine the 2 - D offshore wave envelope spectrum, which are shown in Figures 4.23 and 4.24 for October 10 and 15, respectively. Offshore wave groups with distinct frequencies and cyclic longshore wavenumbers are evident wherever a strong peak of energy occurs.

Viewing figure 4.23, sharp energy peaks indicate highly energetic wave

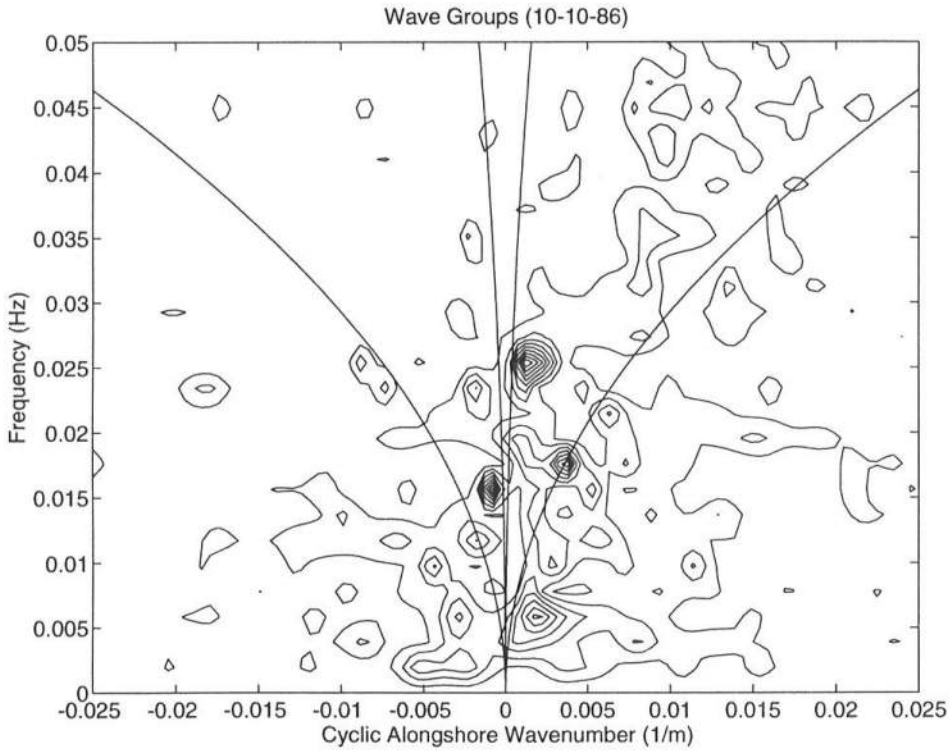


**Figure 4.23:** MLM estimate of the wavenumber-frequency spectra of offshore wave groups for the final 85.33 minutes of data collected on 10-10-86. Theoretical mode 0 edge wave dispersion curves for an effective plane beach slope of 0.055, and the leaky-trapped ($\sigma^2 = gk$) boundary are plotted. Using all offshore pressure data except LA03 and LA10 that are not part of a linear array. 20 D.O.F., $\Delta f = .002$.

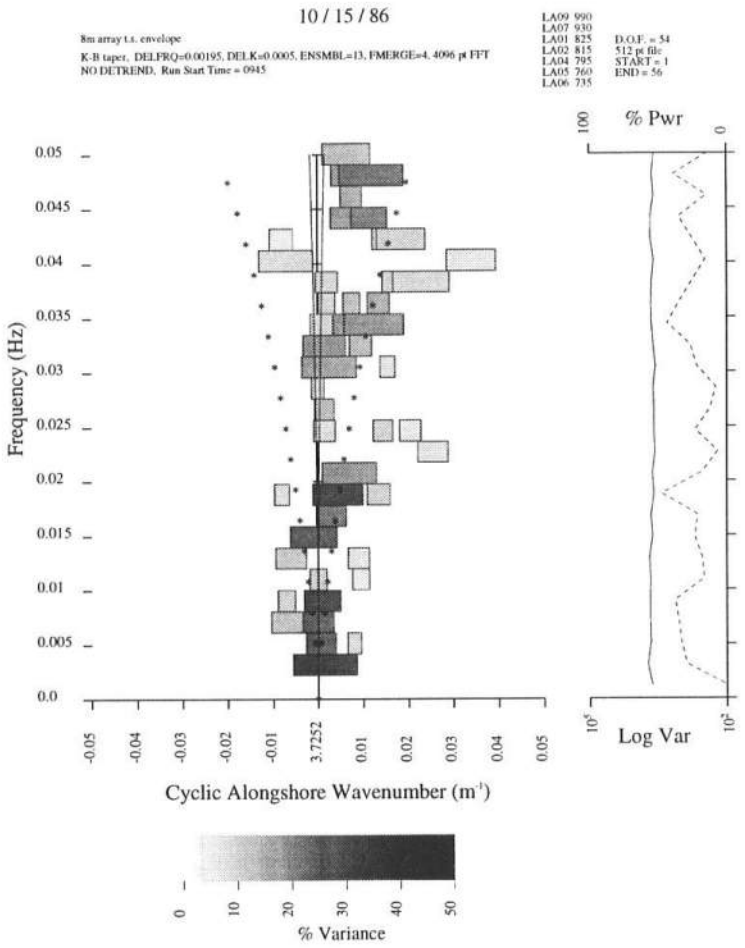


**Figure 4.24:** MLE wavenumber-frequency spectra of offshore wave groups for 10-15-86 @09:45 EST. Positive (negative) wavenumbers indicate southward (northward) propagation. The rectangular boxes mark the location of variance peaks defined as those wavenumber maxima that have an adjacent valley below their half-power. The wavenumber width of each box is the half-power bandwidth of the peak. The shading density indicates the percent variance in the frequency bin that lies within the half-power bandwidth of the peak. Theoretical mode 0 edge wave dispersion curves for an effective plane beach slope of 0.055, and the leaky-trapped ($\sigma^2 = gk$) boundary are plotted. Using all offshore pressure data except LA03 and LA10 that are not part of a linear array. 54 D.O.F., $\Delta f = .002$. Obtained from Dr. Joan Oltman-Shay.

groups near 0.002 and 0.005 $Hz$, existent at the offshore wavegage array. Corresponding cyclic longshore wavenumbers for these wave groups surround $-0.0025$ and 0.0025 $(m^{-1})$, indicating alongshore wave lengths of 400 meters. Referring to Figure 4.8, surf zone velocity motions were observed with a similar frequency and wavenumber as the wave groups with positive alongshore wavenumber. Figure 4.8 illustrates energetic longshore current variations at frequencies of 0.001 through 0.015 $Hz$, with cyclic longshore wavenumbers ranging from 0.0025 to 0.012 $m^{-1}$. Comparing Figures 4.23 and 4.8, there is an obvious correspondence in the longshore wavelengths and relative magnitude of energy between the very low frequency wave groups and surf zone cross-shore velocities. Since similar incident wave groups existed, it is expected the strong 0.001 - 0.005 $Hz$ current oscillation, with cyclic wavenumber around 0.0025 $m^{-1}$, is a result of wave groups providing the perturbation and possible resonant forcing for an exponentially growing shear wave.

Figure 4.24 indicates offshore wave groups in the October 15, 1986 data at a frequency near 0.002 $Hz$ with cyclic longshore wavenumbers ranging from $-0.005$ to 0.008 $m^{-1}$. These wave groups are incident at both normal and oblique angles to the shoreline. The normally incident wave groups are indicative of surf beat, while the obliquely directed wave group, provides potential forcing for low frequency oscillations in the longshore current. Comparing Figures 4.9 and 4.24 reveals energetic offshore wave groups as a probable forcing mechanism for the 0.002 $Hz$ longshore current oscillation with a cyclic alongshore wavenumber of 0.005 $m^{-1}$.

Similarities in the spatial structure of the offshore wave groups and surf zone velocity oscillations are investigated by plotting their phase as a function of longshore gage spatial lag in Figures 4.25 to 4.28. For both of the data sets

studied, these phase comparisons span the range of very low frequencies where oscillating current motions are most energetic. Due to the randomness of the offshore wave field and the transformations incurred as the waves and groups propagate 800 meters into the surf zone, any coherent phase relation between the offshore groups and nearshore velocities is truly remarkable.

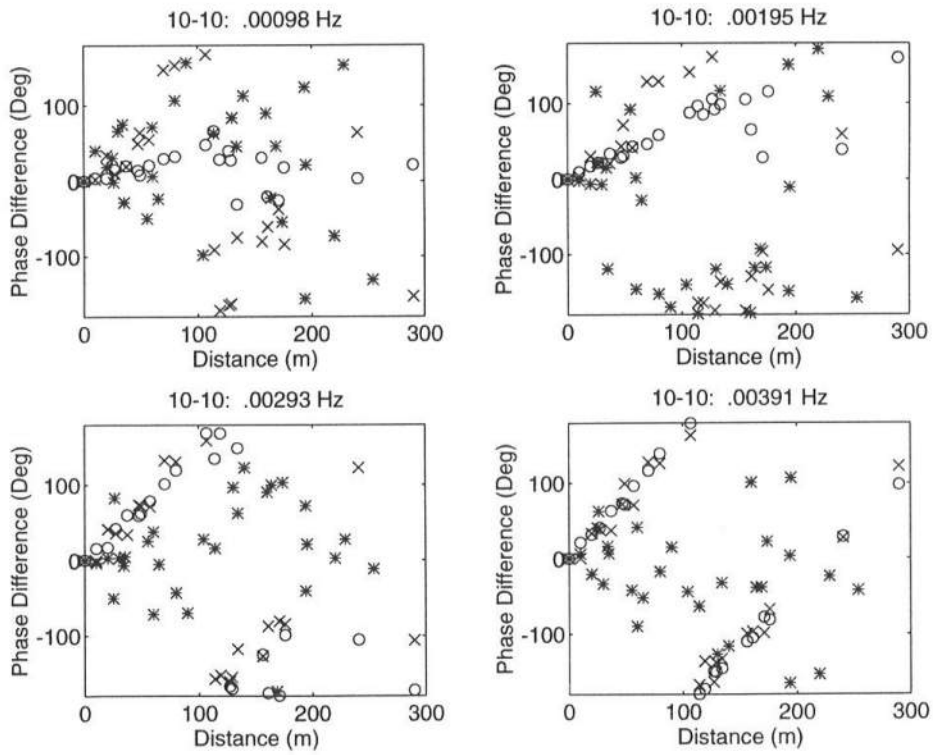


**Figure 4.25:** Phase versus longshore spatial lag for offshore wave groups (*), longshore surf zone velocities (o), and cross-shore velocities (x) for the final 85.33 minutes of data collection on 10-10-86 beginning at 04:00 EST. 26 D.O.F., $\Delta f = 0.001\ Hz$.

Most obvious from Figures 4.25 through 4.28 is the consistently coherent spatial structure of the horizontal oscillations to the longshore current. Often the phase lag of the longshore and cross-shore currents are equal for the longshore gage positions, and the alongshore periodicity of the current oscillations is

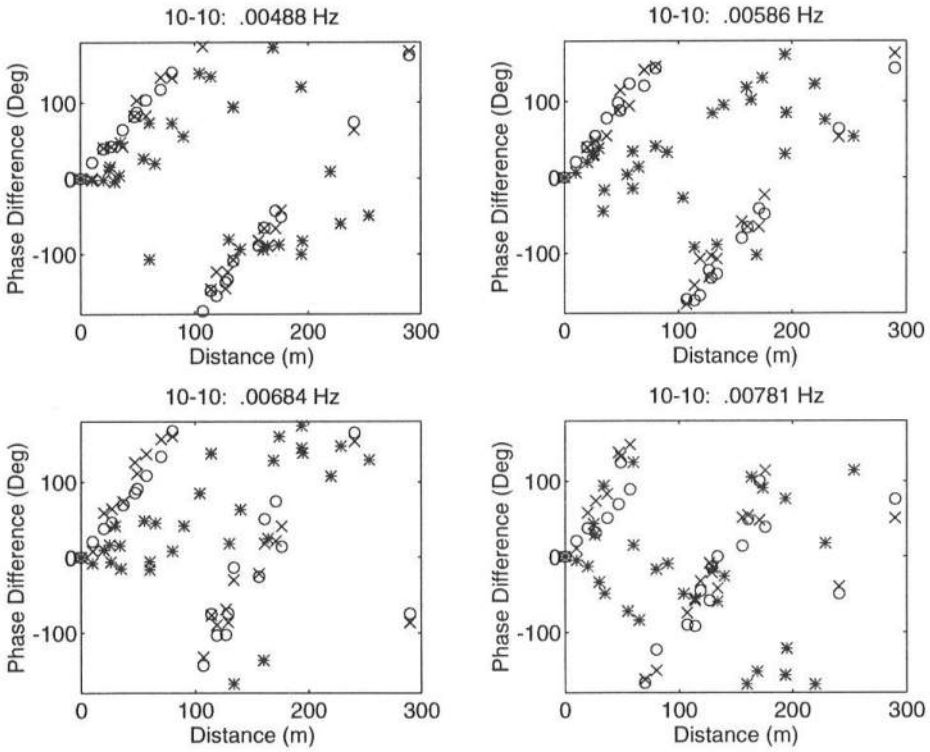


**Figure 4.26:** Phase versus longshore spatial lag for offshore wave groups (*), longshore surf zone velocities (o), and cross-shore velocities (x) for the final 85.33 minutes of data collection on 10-10-86 beginning at 04:00 EST. 26 D.O.F., $\Delta f = 0.001\ Hz$.

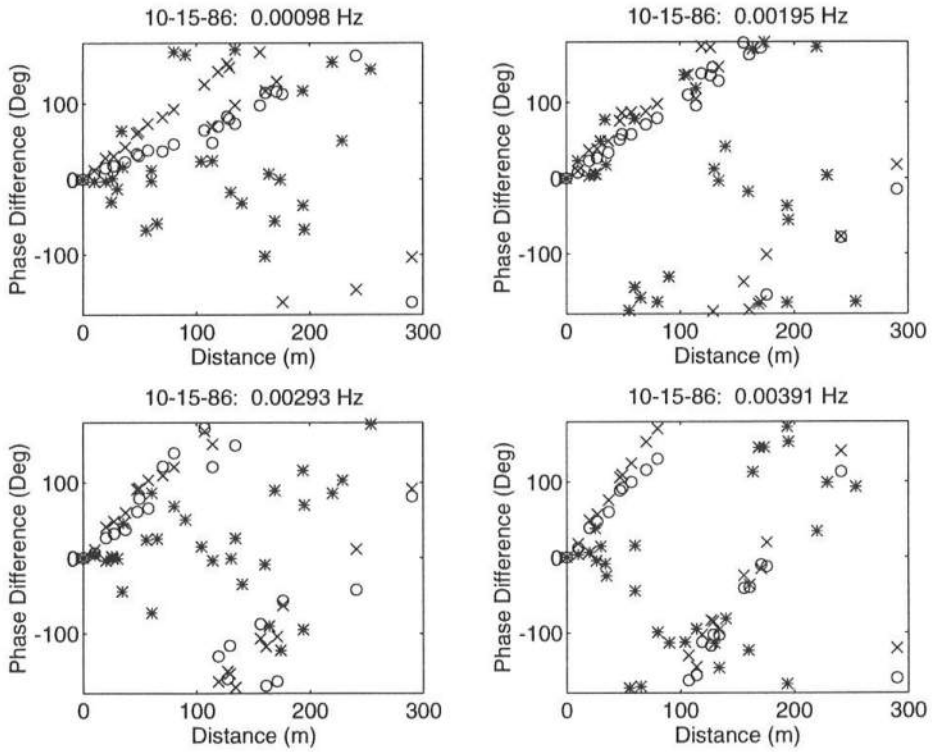


**Figure 4.27:** Phase versus longshore spatial lag for offshore wave groups (*), longshore surf zone velocities (o), and cross-shore velocities (x) for 10-15-86, 09:45 EST. 26 D.O.F., $\Delta f = 0.001\ Hz$.

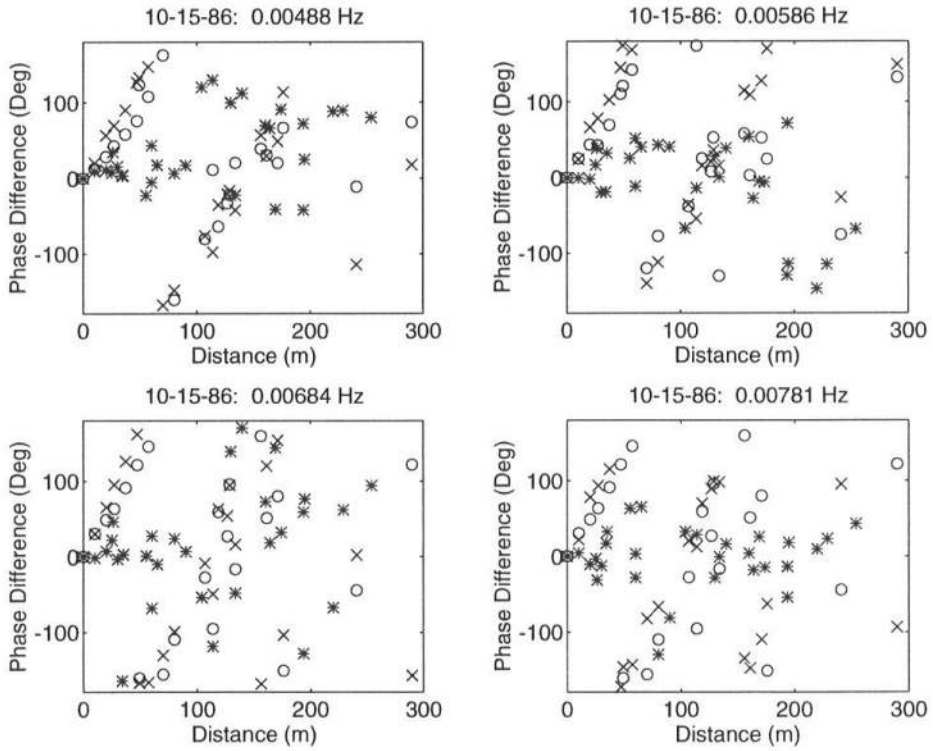


**Figure 4.28:** Phase versus longshore spatial lag for offshore wave groups (*), longshore surf zone velocities (o), and cross-shore velocities (x) for 10-15-86, 09:45 EST. 26 D.O.F., $\Delta f = 0.001\ Hz$.

evident as phase ranges from $-180$ to $+180$ degrees in a linear fashion. The corresponding offshore wave groups are not as spatially coherent, and this is expected. Even so, there is some spatial correlation between the groups and the velocities for particular frequencies. Most notable is the 0.00488 $Hz$ motion, depicted in Figure 4.26, for the October 10 data where there are incident wave groups with longshore structure identical to the surf zone current oscillations. This provides strong evidence of wave group forcing of the low frequency surf zone motion. The general lack of similarity between the wave group and velocity phasing is due, in part, to the randomness in the wave field. For example, for a given frequency, there are obliquely incident wave groups from different angles as well as normally incident surf beat, and the superposition of these motions will have a random phase structure in the longshore.

Again, it is not mandatory that the group structure match that of the current motions for the wave groups to provide the perturbations that initiate velocity oscillations with temporal growth. This correspondence is required for the formation of migrating rip currents or any resonant forcing of unstable motions.

### 4.3.5 Longshore Current Structure Using the Theory of Intersecting Waves

While significant wave groupiness may be due to the frequency spreading of the most energetic incident waves from similar directions, additional wave group structure is provided by the intersections of waves incident from opposite directions. The longshore wavelength, $L_{gy}$, and propagation speed, $C_{gy}$, of these wave groups may be estimated if the directionally spread, bimodal incident wave climates, illustrated in Figures 4.17 to 4.20, are schematized to a superposition of two linear waves incident from different directions. Equations (1.4) and (1.5) for

computing $L_{gy}$ and $C_{gy}$ were developed by Fowler and Dalrymple (1990) for intersecting wave trains of equal amplitudes, causing wave group induced migrating rip currents in the surf zone. As evident from Figures 4.17 and Figure 4.20, the heights of the schematized bi-directional waves are not equal because of the varying magnitude of total power associated with the bimodal groupings of energy. This complication implies a wave group induced meandering current pattern is formed from the superposition of this migrating rip current field with a longshore current. The linear superposition of these two sources of energy is best described by Equation (1.2).

Viewing the direction-frequency wave spectra, extreme direction and frequency spreading is evident, making the necessary simplification of the wave climate difficult. It is expected the wave groups result from the combination of all the spectral component waves as well as their non-linear interactions. However, using pairs of linear wave trains spanning the region of energy spreading will result in a range of longshore wavelengths and propagation speeds that can be compared to the properties of the velocity oscillations measured in the surf zone. Numerous combinations of waves are selected to span the spectra for the two days of interest. The field data comparison for $C_{gy}$, as existent in the surf zone, is simply calculated from the slope of the line of energy representing the nondispersive motion in Figures 4.8 and 4.9. Meanwhile, the range of $L_{gy}$ is determined from the $k_{y,cyc}$ axis of the same figure where significant energy is present. These results are summarized in Table 4.2 so a comparison can be made between the theory and the observations from the MLM analysis of the field data. It is evident the simplified theory reasonably estimates the measured surf zone motion, and bi-directional incident wave groups are a significant forcing mechanism.

**Table 4.2:** Comparison of longshore wavelength and propagation speed of the surf zone current oscillations. S and N denote Southward and Northward directions of propagation, respectively.

| | Field Data | | Prediction | |
|---|---|---|---|---|
| | $C_{gy}$ (m/s) | $L_{gy}$ (m) | $C_{gy}$ (m/s) | $L_{gy}$ (m) |
| 10-10-86 | 1.6 S | 50 - 200 | 0.9 N - 1.8 S | 20 - 45 |
| 10-15-86 | 1.1 S | 50 - 400 | 0.5 S - 4.1 S | 40 - 470 |

## 4.4 Identification of Distinct Edge Waves

There is a large amount of energy depicted in the wavenumber-frequency plots for the surf zone velocities and wave groups that satisfies the dispersion relation for particular modes of edge waves. Visual comparison of these figures indicates a strong relation also exists between the offshore wave group structure and nearshore motions in this higher band of frequencies, the infra-gravity band, as well. For example, Figure 4.24 indicates an incident offshore wave group, near a frequency of 0.017 $Hz$, satisfying the mode 0 edge wave dispersion relation. Further, Figure 4.29 demonstrates a definitive relation between the alongshore phase difference, hence spatial structure, of this wave group and the longshore surf zone velocity. This wave group forcing of edge waves is well documented in the literature (see Section 1.2), and is mentioned here to show the distinction between edge waves, in the infragravity (IG) frequency band (frequencies of $O(10^{-2}-10^{-1})$, and the non-dispersive longshore current oscillations in the far-infragravity (FIG) frequency band (frequencies of $O(10^{-3} - 10^{-2})$.

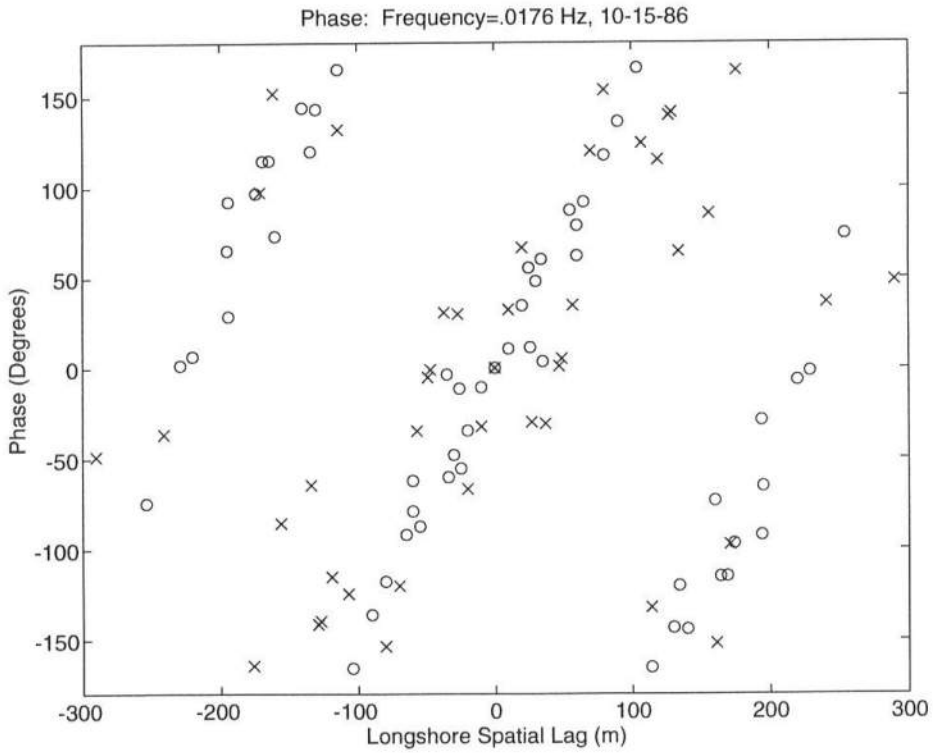


**Figure 4.29:** Phase versus longshore spatial lag for offshore wave groups (o) and longshore surf zone velocities (x) for 10-15-86, 09:45 - 13:45 EST. 26 D.O.F., $\Delta f = 0.001\ Hz$.

# Chapter 5

# PROPOSED LABORATORY EXPERIMENT

When formulating the shear wave theory, Bowen and Holman (1989) supposed, "...for shear wave magnitudes of up to 50% of the peak longshore current, the resulting pattern (is) indiscernible by eye... Thus wave tank experiments may in fact be contaminated with shear wave motions..." Further, Putrevu and Svendsen (1992) argue, "...shear wave motions could be detectable in a laboratory..." Presently, however, there are no documented laboratory observations of shear waves. On the other hand, wave group-forced migrating rip currents have been validated in the laboratory by Fowler and Dalrymple (1990), and this poses a question of the efficacy of shear waves relative to wave groups in the forcing of natural surf zone motions.

To answer this question, a laboratory experiment is proposed to model a natural surf zone, and to determine the importance of wave groups and shear instabilities in the longshore current as sources of low frequency surf zone motion. The model is designed for construction in the directional wave basin at the University of Delaware, where Fowler and Dalrymple (1990) observed the migrating rip currents. This previous work validated the migrating rip current phenomenon for an idealized planar beach and bimodal wave climate with some directional and frequency spreading. It is expected their work can be elaborated to investigate the

effects of barred beach bathymetries, more realistic sea states, such as those measured during SUPERDUCK, and longshore currents induced by incident waves with varying amplitudes.

Scaling arguments are discussed, allowing for a beach that models the natural conditions at SUPERDUCK. A series of controlled test cases are designed to identify migrating rip currents and any instabilities in the longshore current. If these phenomena are successfully modeled, an experimental plan is recommended for identifying the forced wave of vorticity resonance condition between wave groups and shear instabilities. However, if the proposed conditions necessary for instability growth are satisfied and shear waves are not detected, the significance of this phenomenon in nature may be in question. In the most complex case, the experiment should conclude with a "playback" of the incident wave spectrum from SUPERDUCK, and a comparison of the laboratory and field data, testing the accuracy of the model.

## 5.1 Description of the Facility

The experiment will be conducted in the directional wave basin at the University of Delaware. This basin is square, 20 meters on a side, and 1.1 meters deep. Waves are generated via 34 individual paddles, each powered by a one horsepower motor with a position-feedback potentiometer. A Concurrent computer digital-to-analog subsystem sends paddle displacement time series information to each motor through servo-controllers that generate error signals governing the direction and magnitude of paddle motion. Any water surface, from a monochromatic wave train to a realistic sea state with directional and frequency spreading, may be simulated in the basin. For specific information regarding the operation of the basin, one should refer to the user's manual developed by Chawla and Kirby

(1994).

## 5.2 Dynamic Similitude

The Froude number is used to develop scaling relationships between spatial and temporal variables for coastal experiments because of the necessity for dynamic similitude among the dominant forces, inertia and gravity. For an undistorted model, where horizontal and vertical spatial scales are equal, the following relation between model to prototype ratios governs the scaling:

$$t_r = \sqrt{l_r}, \tag{5.1}$$

where $t_r = t_m/t_p$ is the time ratio, and $l_r = l_m/l_p$ is the spatial ratio. Specifying a model to prototype length scale allows for a determination of the corresponding time and velocity scales.

## 5.3 The Viscous Threshold for Shear Wave Development

Shear instabilities in the longshore current may be indetectible in laboratory experiments because bottom friction effects are amplified when the model is scaled. Unless these scaling effects are accounted for, damping of shear wave growth may be expected.

To combat the adverse effects of bottom friction in the lab, Putrevu and Svendsen (1992) proposed a viscous threshold that must be overcome for the instabilities to propagate. These authors recognized, if the bottom friction is assumed to be balanced by the radiation stress, the stability equation (2.18) reduces to:

$$\left(V - c_p - \frac{i\lambda}{kh}\right)\left(\Psi_{xx} - \Psi k^2 - \frac{\Psi_x h_x}{h}\right) - \Psi h\left(\frac{V_x}{h}\right)_x = 0, \tag{5.2}$$

where $\lambda = fV$ is determined from a quadratic relation for the bottom shear stress, $f$ is a friction coefficient, and $V$ is the steady longshore current that may be approximated by the quantity, $V_{max}/2$. The terms within the first pair of parentheses may be rewritten as:

$$V - \frac{\sigma_{re}}{k} - i\left(\frac{\sigma_{im}}{k} + \frac{\lambda}{kh}\right), \tag{5.3}$$

providing a criterion that must be satisfied for the motion to be unstable:

$$\sigma_{im} + \frac{\lambda}{h} < 0, \tag{5.4}$$

or:

$$-\sigma_{im} > \frac{fV}{h} = \sigma_{thresh}, \tag{5.5}$$

where $\sigma_{thresh}$ is a stabilizing threshold, calculable for given experimental values of $f$, $V$, and $h$.

Figures 5a and 6a from Putrevu and Svendsen (1992), repeated in Figure 5.2, allow for computation of typical values of $\sigma_{im}$ for a planar beach, and for barred beaches with varying bar crest positions relative to the wave breaking point, $x_c/x_o$. Figure 5.1 illustrates the beach profiles used by these authors. These figures show numerically computed curves of $\sigma_{im}x_o/V_{max}$ versus $kx_o$ for varying beach profiles, where $x_o$ is the break point, $V_{max}$ is the maximum longshore current, and $k$ is the alongshore shear wavenumber. Given typical values for $kx_o$ and experimental measurements for $x_o$ and $V_{max}$, $\sigma_{im}$ may be interpolated from Figure 5.2 for comparison to experimental $\sigma_{thresh}$, as computed form Equation (5.5). Effective use of these guidelines will allow for a check on the satisfaction of the viscous threshold, and for a laboratory experiment to be "tuned" for optimal shear wave growth conditions.

Representative values for $k$ from SUPERDUCK are obtained by reviewing Figures 4.8 and 4.9, where a typical range of cyclical alongshore wavenumbers for

**Figure 5.1:** The depth variations used. From Putrevu and Svendsen (1992).

**Figure 5.2:** Variation of $\sigma_{im}$. a) For bottom topographies of Figure 5.1. b) For different bar crest locations. From Putrevu and Svendsen (1992).

**Table 5.1:** Suggested computation of $\sigma_{im}$ for varying beach topographies and longshore currents. $x_o$ and $V_{max}$ are computed form laboratory measurements.

| Beach Profile | Range of $\sigma_{im}\,(x_o/V_{max})$ |
|---|---|
| Plane Slope | $0.0 \Rightarrow 0.13$ |
| Barred Beaches | |
| $x_c/x_o = 1$ | $0.020 - 0.280$ |
| $x_c/x_o = 0.7$ | $0.033 - 0.120$ |
| $x_c/x_o = 0.65$ | $0.410 - 0.075$ |
| $x_c/x_o = 0.6$ | $0.032 - 0.080$ |
| $x_c/x_o = 0.46$ | $0.000 - 0.110$ |

the shear waves with the highest energy is 0.0025 to 0.008 $m^{-1}$. This suggests a range of longshore wavenumber, $k$, of 0.016 to 0.05$m^{-1}$, with associated alongshore wave lengths, $L_y$, of 125 to 400 meters. The wave breaking point is also estimated from SUPERDUCK field observations, and typical surf zone widths, $x_o$, range from 100 to 150 meters. These observed values of $L_y$ and $x_o$ are consistent with the estimates of $L \sim (1-4)x_o$, by Bowen and Holman (1989) and Putrevu and Svendsen (1992). Computing $kx_o$ then specifies a typical range of 1.6 to 7.5.

Using Figure 5.2 with the typical $kx_o$ values, the corresponding range of $\sigma_{im}\,(x_o/V_{max})$ values may be interpolated for various cross-shore beach profiles. Table 5.1 summarizes the results, and may be used as a guideline for satisfying the viscous threshold when conducting laboratory experiments. Using Table 5.1, laboratory measurements of $x_o$ and $V_{max}$ may be used to compute $\sigma_{im}$, which may then be compared to $\sigma_{thresh}$ for a check on the potential growth of shear waves in the experiment.

## 5.4 Appropriate Model Scales

A Froude number model for the SUPERDUCK experiment is governed by the length scale, and is subject to the size constraints imposed by the directional wave basin. A number of physical parameters of the SUPERDUCK field study must be considered when selecting the appropriate model spatial scale.

First, the offshore pressure gage array at SUPERDUCK, spanning 254 meters, may be modeled by the 20 meter long segmented wave maker. Under this criterion, a preliminary estimate for the length scale is $l_r = \frac{20}{254} \approx \frac{1}{13}$. Another consideration for the scale ratio is imposed by the length of the array of surf zone velocity meters from SUPERDUCK, 509 meters. This is important because while shear waves are a temporal instability, there must be a sufficiently long beach for the potential current instabilities to grow to a measurable amplitude, thus $l_r = \frac{20}{509} \approx \frac{1}{25}$ is suggested.

Viscous effects are also of concern, and the scaling must allow for a sufficient depth at breaking, $h_b$, so surf zone motions are not overly damped by viscosity. Specifying a lower limit on the model depth at breaking, $h_{b,min}^{model} = 0.05m$, and considering the breaker depth at SUPERDUCK was $h_b = 1.0$ to $1.5$ meters, the model scaling should be no smaller than $\frac{1}{30}$.

Finally, the spatial scaling may be estimated by modeling the offshore distance of the pressure gage array from SUPERDUCK, which was approximately 800 meters. Conveniently, this would allow for the waves specified at the paddles to equal the waves measured at the offshore pressure gage array at SUPERDUCK. Considering the wavemaker and the beach limit the length of the directional basin to 17 meters, at most, a representative ratio for this model is $l_r = \frac{17}{800} \approx \frac{1}{50}$. However, this scale is small, when considering the surf zone viscosity criteria.

Consequently, when specifying the SUPERDUCK spectrum, measured 800 meters offshore, the effects of shoaling, refraction, and diffraction must be considered, since the wave climate will be specified relatively closer to the shoreline. For shoaling effects only, a response function for the linear shoaling coefficient may be simply computed for a constant sloping beach. If refraction is to be considered or a specific bottom bathymetry is specified, a numerical model, such as REF/DIF 1 (Kirby and Dalrymple, 1993), should be employed for shoaling the spectrum.

The choice of appropriate model scaling is also governed by the beach slope, as well as the expected alongshore wavenumbers of migrating rip currents and potential shear instabilities. A typical shoreline beach slope from SUPERUCK was $0.055 \sim 1:18$, while the slope was nearly $1:100$ seaward of the sand bar. A representative model beach slope is chosen as $1:20$ so that the foreshore is well represented. Using the minimum depth at breaking and considering the resulting surf zone width for a plane beach slope, a reasonable model scale is $\frac{1}{20}$. This results in a minimum model breaker depth of $h_{b,min}^{model} \sim 0.05$ to $0.075$, which is above the specified lower limit for $h_{b,min}^{model} = 0.05m$. A corresponding model surf zone width for the plane beach is estimated as $x_o^{model} \sim 1.0$ to $1.5$ meters; therefore, from Section 5.3, alongshore shear wave lengths are expected to be $k \sim 1.0$ to $6.0$ meters. It is speculated this provides sufficient length for shear wave growth in the 20 meter directional basin. For barred beaches, the surf zone width is governed by the depth and cross-shore position of the bar crest. For bar crests far offshore, wide surf zones allow for longer shear instabilities that may not grow to detectable amplitude. Reviewing Table 4.2, the alongshore distances between the migrating rip currents, for the $\frac{1}{20}$ model, will be scaled to $L_{gy} \sim 2.5$ to $20$ meters, with the shorter range of $L_{gy}$ easily observed in the 20 meter width wave basin.

Interestingly, the model scaling, for a plane beach slope, has conflicting

effects on the predicted wave lengths of shear instabilities and migrating rip currents. Whereas the shear wave lengths are a function of the surf zone width, $x_o$, the rip current spacing is simply related to the spatial scaling, and this is the source of the scaling descrepancy. Effectively, this may allow for the two motions to be distinguished when testing the natural SUPERDUCK data on a planar beach. This scaling difference must be considered when testing for the wave group induced resonance of shear wave motions, which result in forced waves of vorticity. Again, the experiment may be "tuned" by adjusting the surf zone width with the bar crest position, allowing for the shear instabilities and group structure to be scaled similarly. More detail is provided on this topic in Section 5.5.

## 5.5 Proposed Tests

The following proposed tests merely outline a recommended cognitive procedure for investigating shear waves and wave group-induced meandering current patterns in the laboratory. The progression of experiments, from an obliquely incident monochromatic wave on a plane beach slope to a complex frequency and directionally spread incident wave climate incident on a barred beach, should allow for a better interpretation of measured results. Included with the outline of each test is a brief discussion of expected results, justifying the potential scientific gain from the test.

### 5.5.1 TEST 1: Shear Waves on a Planar Slope.

This test involves a simple monochromatic wave train, incident on the $1:20$ planar beach. The choice of wave height and incident angle will be experimentally determined from measurements of longshore currents and surf zone widths. The experiment should be "tuned" so the incident wave generates a sufficient

longshore current, $V_{max}$, breaker depth, $h$, and surf zone width, $x_o$, to satisfy the viscous threshold for shear wave growth (see Section 5.3). Of great importance to this experiment is the value of the friction factor, $f$. Usually, a value of 0.02 is assumed, but this may be a strong underestimate for the lab. To mitigate this discrepancy, the beach bottom in the surf zone should be constructed as smooth as possible using fine grit sandpaper and paint. Next, since shear wave lengths are expected to be a function of the surf zone width, and a sufficient length of beach is required for the instabilities to be detected, $x_o$ is an increasingly important parameter. The surf zone width should be narrow, permitting a few of the expected longest shear wave lengths in the longshore. In any event, initial surf zone velocity measurements should be made at the termination of the alongshore beach so the motion has a larger amplitude.

It is expected that longshore current instabilities will be observed when the viscous threshold is satisfied, and if the motion has space and time to grow. If such motions are measured, these are the first laboratory observations of shear instabilities, and an ensuing detailed investigation of these motions is in order. Attention should be directed to an analysis of the growth rates of the instabilities, and particularly the length and time scales required for growth should be determined.

In the event that the viscous threshold is satisfied and no instabilities are observed, the surf zone width should be reduced to allow for a relatively longer beach for the unstable motions to grow. It is possible, however, that the background vorticity generated on the planar beach at the seaward boundary of the longshore current profile is not strong enough to instigate a measurable instability. In this case, the effects of a barred beach should be investigated.

### 5.5.2 TEST 2: Shear Waves on a Barred Beach.

An offshore bar dramatically increases the background vorticity generated at the seaward boundary of a longshore current profile, and provides a stronger restoring force for shear instabilities to the longshore current. Repeating the wave conditions of TEST 1 on a barred beach will increase the possibility of generating shear waves in the lab. A barred beach is also convenient for "tuning" the experiment because for a given wave breaking on the bar crest, the surf zone width, $x_o$, may be adjusted by repositioning the bar. Examination of the viscous threshold requirements for a barred beach, Table 5.1, reveals a less stringent requirement. Note, Table 5.1 is specific for a bar that reduces the depth at the crest to one-half the corresponding depth on the planar slope.

Again, it is expected that instabilities in the longshore current will be observed when the effects of the bottom friction are overcome, and when the beach length is sufficient for shear wave growth. All observed shear wave motions are significant, and comprehensive data sets should be collected. It is anticipated that growth rates are faster for the barred beach. The significance of shear waves as a natural phenomenon is in question if there are no observed instabilities on the barred beach when the viscous threshold is satisfied.

### 5.5.3 TEST 3: Wave Group Induced Migrating Rip Currents on Planar and Barred Beaches.

Regardless of any shear wave observations in TEST 1 and TEST 2, further laboratory investigation of migrating rip currents is of interest. Two equal amplitude monochromatic waves with slightly different frequencies, incident from different directions, should be selected using Equations (1.4) and (1.5) so the rip

spacing is of appropriate length for measurement in the 20 $m$ basin. Fowler (1991) may be referenced for typical laboratory test cases.

Upon observing migrating rip currents, on a plane beach slope, with $C_{gy}$ and $L_{gy}$ predicted by the theory, the effect of a barred beach should be investigated. As the bar may inhibit the cross-shore flow of the rip current, the significance of migrating rips on a barred beach needs to be validated.

If typical shear wave lengths were observed in the first two tests, combinations of incident waves should be selected to produce migrating rips with $L_{gy}$ equal to the shear wave lengths. This is crucial for testing the potential excitation and resonance of shear waves by the incident wave groups.

### 5.5.4 TEST 4: Wave Group Induced Meandering Current Patterns.

Based on the numerical simulations of Ebersole and Dalrymple (1979), it is proposed that if the amplitude of one of the wave trains described in TEST 3 is increased, the additional energy will be manifested in the form of a steady longshore current. Using superposition principles, which is a simplification due to the nonlinearity of the nearshore circulation system, it is expected that adding the constant longshore current to the migrating rip currents will produce a meandering longshore current pattern. This should be investigated on the barred beach as well as on an idealized planar slope. Surf zone velocity measurements of this motion are indistinguishable from shear waves, neglecting the temporal growth.

This test is a modification of TEST 3, and only requires adjustment of the amplitudes of the incident waves. As with shear waves, there are no previous laboratory observations of this type of motion, so the collection of comprehensive data sets is desired for an investigation of the physics and for the calibration of

numerical models similar to Ebersole and Dalrymple (1979).

### 5.5.5 TEST 5: Wave Group Initiation and Resonance of Shear Instabilities in the Longshore Current.

Provided that shear waves were observed in TEST 1 or TEST 2, and that migrating rip currents can be simulated with $L_{gy}$ equal to the shear wave lengths, TEST 5 is an attempt to superimpose these two phenomena and investigate potential resonance characteristics. Essentially, this test is similar to TEST 4, but the increased amplitude of one of the incident waves must be such that a potentially unstable longshore current is added. The additional longshore current should satisfy the viscous threshold for shear wave growth, and further convenience is gained if the longshore current is equivalent to a current in TEST 1 or TEST 2 where shear waves were observed, and typical shear wave lengths are known. This will allow for the experiment to be "tuned" so that the expected lengths of shear waves and incident wave groups are equal. Equation (1.2) may be utilized to specify two incident planar waves with different amplitudes such that the unmodulated free wave, $(a_1 - a_2)\sin\Psi_2$, is similar to the oblique wave train which initiated a previously observed unstable longshore current.

It is expected that the addition of the resonant wave group structure will increase the growth rate of the instability. The maximum amplitude of the meandering current may also be increased with the additional wave group forcing.

### 5.5.6 TEST 6: SUPERDUCK Field Data Simulation.

Having completed the idealized and controlled experiments described in TESTS 1 - 5, an attempt should be made at reproducing a natural sea state which

is known to have initiated oscillating longshore currents. Based on the directional spectra computed in Chapter 4, the wave climates measured on October tenth and fifteenth, 1986 at the SUPERDUCK field study will be simulated in the laboratory. Surf zone motions induced by these wave climates should be compared to the field observations.

Preliminary tests of the simulated SUPERDUCK wave climate have been performed with encouraging results. The MLM estimated wave spectrum is simplified by assuming a uni-directional wave for each frequency, with the representative direction being computed from a weighted average as follows:

$$\theta(f_n) = \frac{\int_{-\pi}^{\pi} \theta D(f_n, \theta) d\theta}{\int_{-\pi}^{pi} D(\omega, \theta) d\theta}, \tag{5.6}$$

where $D(\omega, \theta)$ is the directional spreading function for each frequency. Since the directional spreading function is normalized, the denominator of (5.6) is unity by definition. It is also required that a wave amplitude be specified for each frequency, and this is computed from the power spectral density value $S(f)$ at each frequency as follows:

$$a(f_n) = \sqrt{S(f_n)\Delta f}, \tag{5.7}$$

where $\Delta f$ is the frequency step in the spectral analysis.

Finally, as wave groupiness may depend on the relative phase of each of the spectral components, this is determined from the phase spectrum as:

$$\phi(f_n) = \tan^{-1} \frac{\Re e \{F_n\}}{\Im m \{F_n\}}, \tag{5.8}$$

where $Fn$ is the Fourier amplitude of the signal from one specified gage. In this experiment, gage LA09 was specified to govern the relative phasing between the component wave trains. This is in contrast to the usually assumed random phase, and is expected to produce a better result in simulating the wave climate measured in the field.

The preliminary tests were conducted in the wave basin for a constant 0.77 meter water depth with an energy dissipating rock beach. The amplitude and period of the specified waves were scaled according to the Froude number with a $\frac{1}{20}$ length scale.

Figures 5.3 and 5.4 illustrate the MLM estimate of the directional spectrum as measured in the wave basin. Visual comparison of these figures shows that the wave climate measured in the field has been reproduced well, qualitatively, in the laboratory. Essentially, the energy peak is at the correct scaled frequency, the mean directions are comparable, and even the directional spreading compares well to the field conditions.

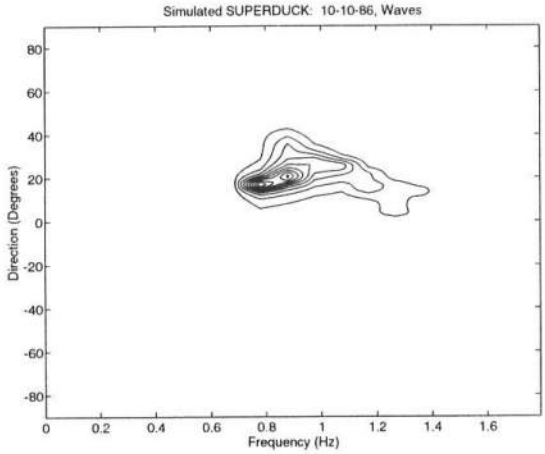


**Figure 5.3:** MLM estimated two-dimensional wave spectrum from the laboratory data simulating the SUPERDUCK wave climate for the final 85.33 minutes of data collected on 10-10-86. Contours represent tenths of peak power. 80 D.O.F., $\Delta f = 0.097\ Hz$.

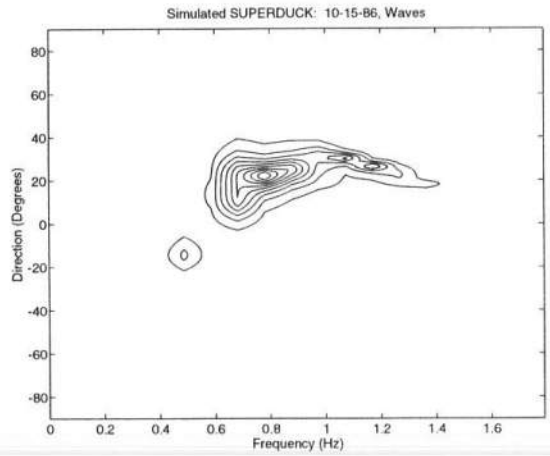


**Figure 5.4:** MLM estimated two-dimensional wave spectrum from the laboratory data simulating the SUPERDUCK wave climate on 10-15-86. Contours represent tenths of peak power. 64 D.O.F., $\Delta f = 0.097 Hz$

Further, the laboratory data was analyzed for the existence of low frequency wave groups, and the MLM estimated frequency versus cyclical alongshore wavenumber spectra are illustrated in Figures 5.5 and 5.6. Here, the existence of obliquely incident low frequency wave groups is evident. Also encouraging is the alongshore wavenumbers associated with these wave groups, which scale to similar values as the wave groups observed in the field. However, for scaled frequencies corresponding to the very low motions in the field ($\leq 0.005\,Hz$ in the field scales to $\leq 0.02\,Hz$ in the lab), the laboratory wave groups are more normally directed. This may be due to the lack of resolution in the spectral analysis at these very low frequencies. For example, for the field data the frequency step of .00098 Hz allowed for five discretized frequencies less than $0.005\,Hz$, whereas the frequency step for the analysis of laboratory data was $0.049\,Hz$ and does not even resolve one frequency within the scaled range. Nonetheless, the preliminary laboratory tests illustrate that obliquely incident low frequency wave groups are present.

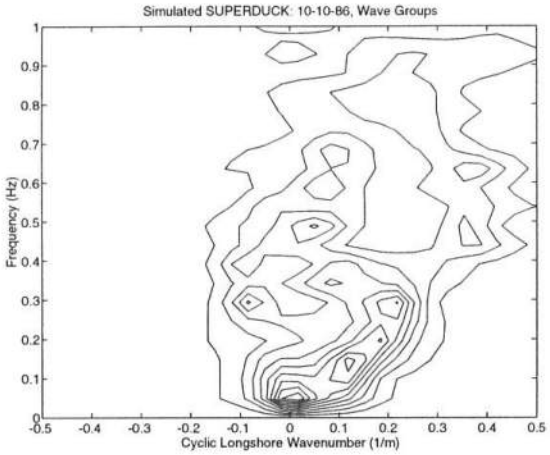


**Figure 5.5:** MLM estimated two-dimensional wave group from the laboratory data simulating the SUPERDUCK wave climate for the final 85.33 minutes of data collected on 10-10-86. Power is normalized to unity for each frequency bin. Contours represent tenths of peak power. 40 D.O.F., $\Delta f = 0.049\ Hz$.

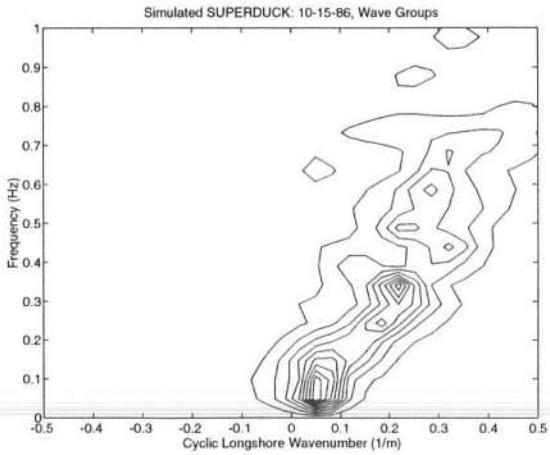


**Figure 5.6:** MLM estimated two-dimensional wave group from the laboratory data simulating the SUPERDUCK wave climate for 10-15-86. Power is normalized to unity for each frequency bin. Contours represent tenths of peak power. 40 D.O.F., $\Delta f = 0.049\ Hz$.

### 5.5.7 General Notes

The tests should be conducted on a 1:20 planar sloping beach that can be converted to a barred beach. The bar should be uniform in the longshore, and adjustable so the bar crest location may be repositioned to change the wave breaking point. Generally the depth at the bar crest, $h_c$, should be one half of the planar beach depth, at the same cross-shore location, to match the conditions for which the viscous threshold was calculated by Putrevu and Svendsen (1992).

The basin water depth should allow for the incident waves to be in "deep water" at the seaward toe of the slope, so that refraction on a constant slope may be used in the wavemaker theory (see Dalrymple (1988)).

As fast longshore currents will be generated, a significant recirculation pattern is expected in the basin, which may contaminate the experiments. Truncation of the beach short of the sides of the basin, or the construction of a wall similar to Fowler (1991) may inhibit the development of these recirculation patterns. Alternatively, in the case of shear wave growth, a recirculation pattern may contribute to a better model, because in effect there is an upcoast source of longshore current. Measurements of the mean longshore current at the upcoast and downcoast ends of the beach may, in fact, indicate a need for additional pumping of water from downcoast to upcoast to maintain a constant longshore current.

For reliable estimates of surf zone dynamics, the velocities should be measured for at least four positions in the longshore, with a spatial lag of 2,3,1. To avoid spatial aliasing, the unit distance should be one half of the shortest expected shear wave or longshore rip current spacing. When measuring the migrating rip currents, Fowler (1991) used only two bi-directional velocity meters. Assuming

the experiments were repeatable, the velocity meters were repositioned for successive experiments with the same wave climate, and all of the velocity records were analyzed as if measured during one experiment. Since shear waves are a time-dependent phenomenon, the "repeatability" of the experiments must be verified if only two velocity meters are used for these tests.

Finally, the data should be analyzed similar to Chapter 4 of this thesis. Computer programs for this type of spectral analysis are available in Hamilton and Dalrymple (1994).

# Chapter 6

# SUMMARY AND CONCLUSIONS

Initiated as a data analysis designed to aid in the development of a laboratory experiment for the simulation of the natural conditions from the SUPERDUCK field study, this work has led to a better physical understanding of low frequency surf zone motions. Most notable is the relation between the structure of incident short wave groups and the nearshore circulation patterns. This was revealed through a close examination of the offshore wave data, corresponding to times when unique low frequency horizontal current oscillations, previously attributed to shear waves, were active. An ensuing reformulation of the shear wave theory including the effects of wave groups verifies the hypothesis that wave groups are significant in the forcing of shear instabilities or similar motions in nature.

Support for this phenomenon is provided through analysis of the data from the SUPERDUCK field experiment. Using the MLM and MEM and the data from the linear offshore wave gauge array, the direction-frequency spectra of the incident waves is shown to have frquency and directional spreading of energy, and to have a bimodal structure when the low frequency surf zone motions occur. This energy spreading and bimodal structure of the incident wave spectrum indicates the presence of wave groups, which is verified by calculating the groupiness factor and the Hilbert transform of the transformed (to the water surface elevation)

pressure data. Additional analysis of the Hilbert transform, with the MLM, has allowed for the identification of specific incident wave groups with frequencies and cyclic longshore wavenumbers corresponding to those of the surf zone motions. Plotting the phase of these offshore wave groups and the phase of the surf zone velocity motions versus longshore gage position has shown their spatial structure is nearly the same. Therefore, it is concluded, for the SUPERDUCK field experiment, that incident wave groups provided a forcing mechanism for the observed low frequency surf zone dynamics.

Spurred by these field observations, an expansion of the theory governing low frequency horizontal oscillations of the longshore current to include radiation stress effects from incident wave groups indicates these surf zone velocity variations can be forced by the wave climate. A governing equation is developed that shows how incident wave groups force finite amplitude horizontal oscillations to the longshore current, resulting in a forced wave of vorticity, irrespective of any instability. These motions can also be maintained through the restoring force provided by the conservation of vorticity. Further, incident wave groups with longshore spatial structure similar to shear waves provide the perturbations necessary to initiate shear instabilities. Prolonged wave group forcing serves as a type of resonant forcing for these oscillations, potentially affecting the growth rate and maximum amplitude of the temporally unstable motions.

This increased physical understanding of low frequency surf zone motions raises a series of more specific questions to be investigated in future work. As a priority, the equation governing the vorticity balance with wave group radiation stress forcing must be solved. Analytical and numerical solutions will provide details about the significance of the wave group-forced motions. Presently, Hamilton

et al. (1994) have presented a simplified numerical solution for a flat bottom, bi-linear velocity profile as described by Bowen and Holman (1989), and radiation stress forcing as presented by Bowen (1969). This verifies the existence of group-forced horizontal current oscillations. An analytical solution to this problem is also being investigated.

Future work should also be devoted to investigating the relative sizes of the wave group-induced motions versus the shear waves, and the temporal growth rates of the motions. Discussions with Dr. Joan Oltman-Shay indicate that a comparison of the maximum growth rates and rates of energy transfer of the shear intabilities to those of the vorticity waves resonantly forced by the wave groups will provide an answer to this question. Additionally, to develop an estimate of the relative strengths of these two different processes, a scaling comparison between the perturbations of the background vorticity and the radiation stresses may be analyzed.

Finally, there is the fundamental question of "which comes first?" the shear instability or the wave group-induced motion. This can not be distinguished from the field data, but as discussed in Section 4.3.2.2, there is evidence that shear waves may "spin-up" in the presence of wave groups. The best way to answer this question is through an experimental laboratory procedure similar to the outline presented in Chapter 5, from which conclusions can be drawn about the necessary conditions for low frequency horizontal current oscillations to develop.

# REFERENCES


Bendat, J. S., and A. G. Piersol (1986). *Random Data Analysis and Measurement Procedures.* $2^{nd}$ Edition, John Wiley and Sons.

Bowen, A. J. (1969). "Rip Currents: 1. Theoretical Investigations." *Journal of Geophysical Research*, 74, 5,467-5,478.

Bowen, A. J., and R. T. Guza (1978). "Edge Waves and Surf Beat." *Journal of Geophysical Research*, 83, C4, 1,913-1,920.

Bowen, A.J., and R.A. Holman (1989). "Shear Instabilities of the Mean Longshore Current," 1. Theory. *Journal of Geophysical Research*, 94, 18,023-18,030.

Capon, J. (1969). "High-Resolution Frequency-Wavenumber Spectrum Analysis." *Proc. IEEE*, 57, 1,408-1,418.

Capon, J., R.J. Greenfield, and R.J. Kolker (1967). "Multidimensional Maximum-Likelihood Processing of a Large Aperature Seismic Array." *Proc. IEEE*, 55, 192-211.

Chawla, A., and J. T. Kirby (1994). Documentation for Operating the Directional Wave Basin. Manuscript in preparation, CACR.

Dalrymple, R. A. (1988). "Directional Wavemaker Theory with Sidewall Reflection." *Journal of Hydraulic Research*, 27, 1, 23-34.

Dalrymple, R. A. (1975). "A Mechanism for Rip Current Generation on an Open Coast." *Journal of Geophysical Research*, 80, 3,485-3,487.

Davis, R. E., and L. A. Regier (1977). "Methods for Estimating Directional Wave Spectra from Multi-Element Arrays." *Journal of Marine Research*, 35, 453-477.

Dean, R. G., and R. A. Dalrymple (1991). *Water Wave Mechanics for Engineers and Scientists.* Advanced Series on Ocean Engineering - Volume 2, World Scientific Publishing Co. Pte. Ltd.

Dodd, N., J. Oltman-Shay, and E.B. Thornton (1992). "Shear Instabilities in the Longshore Current: A Comparison of Observation and Theory." *Journal of Physical Oceanography*, 22, 1, 62-82.

Ebersole, B. A., and R. A. Dalrymple (1979). "A Numerical Model for Nearshore Circulation Including Convective Accelerations and Lateral Mixing." Ocean Engineering Report No. 21, Department of Civil Engineering, University of Delaware.

Eckart, C. (1951). "Surface Waves on Water of Variable Depth." *Wave Rep. 100*, 99 pp., Scripps Inst. of Oceanogr., Univ. of Calif., La Jolla.

Fowler, R. E. (1991). "Wave Group Forced Nearshore Circulation: A Generation Mechanism for Migrating Rip Currents and Low Frequency Motion." Final Report, NSF # MSM 8712203. Research Report No. CACR-91-03, Center for Applied Coastal Research, University of Delaware, Newark, Delaware.

Fowler, R. E., and R. A. Dalrymple (1990). "Wave Group Forced Nearshore Circulation." *Proc. 22nd Int. Coastal Engrg. Conf.*, ASCE, 729-742.

Funke, E.R., and E.P.D. Mansard (1979). "On the Synthesis of Realistic Sea States." *Hydraulics Laboratory Technical Report LTR-HY-66*, National Research Council of Canada.

Funke, E.R., and E.P.D. Mansard (1980). "On the Synthesis of Realistic Sea States." *Proc. 17th Int. Coastal Engrg. Conf.*, ASCE, 2,975-2,991.

Gallagher, B. (1971). "Generation of Surf Beat by Non-linear Wave Interactions." *J. Fluid Mech.*, 49, 1-20.

Greenberg, M. D. (1988). *Advanced Engineering Mathematics.* Prentice Hall, Englewood Cliffs, New Jersey.

Hamilton, R.P. Jr., and R.A. Dalrymple (1994). "Computing Two-Dimensional Wave Spectra from an Array of Wave Gauges: Application of the Maximum Likelihood and Maximum Entropy Methods." CACR Report.

Hamilton, R.P. Jr., R.A. Dalrymple, J. Oltman-Shay, and U. Putrevu (1994). "Wave Group Forcing of Low Frequency Surf Zone Motion." Manuscript in preparation.

Huntley, D.A., R.T. Guza, and E.B. Thornton (1981). "Field Observations of Surf Beat 1. Progressive Edge Waves." *Journal of Geophysical Research*, 86, C7, 6,451-6,466.

Isobe, M., and K. Kondo (1984). "Method for Estimating Directional Wave Spectrum in Incident and Reflected Wave Field." *Proc. 19th Int. Coastal Engrg. Conf.*, ASCE, 467-483.

Kirby, J. T. (1993). *Analysis of Regular and Random Ocean Waves: Notes for CIEG 681.* Center for Applied Coastal Research, University of Delaware.

Kirby, J. T., and R. A. Dalrymple (1993) "Combined Refraction/Diffraction Model: REF/DIF 1 Version 2.4 Documentation and User's Manual" Report No. CACR-92-04, Center for Applied Coastal Research, University of Delaware, Newark, Delaware.

Lamb, Sir Horace (1932). *Hydrodynamics.* Sixth Edition, Dover Publications, New York.

LeBlond, P.H., and L.A. Mysak (1978). *Waves in the Ocean.* Elsevier Scientific Publishing Company, New York.

Longuet-Higgins, M.S. (1970). "Longshore Currents Generated by Obliquely Incident Sea Waves." *Journal of Geophysical Research*, 75, 644-663.

Longuet-Higgins, M.S., and R.W. Stewart (1964). "Radiation Stresses in Water Waves: A Physical Discussion, with Applications." *Deep Sea Research*, 11, 529-562.

Mase, M., Takao Yamashita, and Katsuyuki Hayashi (1990). "Wave Group Properties of Coastal Waves." *Proc. 22nd Int. Coastal Engrg. Conf.*, ASCE, 177-190.

Munk, W. H. (1949). "Surf Beats." *Trans. Am. Geophys. Union*, 30, 849-854.

Nakamura, and Katoh (1992). "Generation of Infragravity Waves in Breaking Process of Wave Groups." *Proc. 23rd Int. Coastal Engrg. Conf.*, ASCE, 990-1,003.

Nwogu, O. (1989). "Maximum Entropy Estimation of Directional Wave Spectra from an Array of Wave Probes." *Applied Ocean Research*, 11, 4, 176-182.

Oltman–Shay, J., P.A. Howd, and W.A. Birkemeier (1989). "Shear Instabilities of the Mean Longshore Current," 2. Field Observations. *Journal of Geophysical Research*, 94, 18,031-18,042.

Pawka, S.S. (1983). "Island Shadows in Wave Directional Spectra." *Journal of Geophysical Research*, 88, C4, 2,579-2,591.

Putrevu, U., and I. A. Svendsen (1992). "Shear Instability of Longshore Currents: A Numerical Study." *Journal of Geophysical Research*, 97, 7,283-7,303.

Radin, S. H., and R. T. Folk, Lehigh University, (1982). *PHYSICS for Scientists and Engineers.* Prentice-Hall, Inc., Englewood Cliffs, New Jersey.

Seymour, R. J. (1989). *Nearshore Sediment Transport.* Plenum Press, New York.

Shannon, C. E., and W. Weaver (1949). *The Mathematical Theory of Communication.* The University of Illinois Press: Urbana.

Smith, J. M., and J. M. Kaihatu (1989). *Estimation of Directional Wave Spectra: Direct Fourier Transform Method vs. Maximum Likelihood Method.* Term Project for CIEG 681, University of Delaware.

Stokes, Sir G.G. (1846). "Report on Recent Researches in Hydrodynamics." *Brit. Ass. Rep.*, [*Papers*, i. 167].

Tang, E. C.-S., and R. A. Dalrymple (1989). "Nearshore Circulation: Rip Currents and Wave Groups." *Nearshore Sediment Transport Study*, R.J. Seymour ed., Plenum Press.

Tucker, M.J. (1950). "Surf Beats: Sea Waves of 1 to 5 Minute Period." em Proc. Royal Soc., A202, 565-573.

Ursell, F. (1952). "Edge Waves on a Sloping Beach." *Proc. Roy. Soc. London, Ser. A*, 214, 79-97.

Wylie, C. R., and L. C. Barrett (1982). *Advanced Engineering Mathematics.* Fifth edition, McGraw-Hill International Book Company, Tokyo.

Yu, Yu–xiu, and Shu–xue Liu (1990). "The Group Characteristics of Sea Waves." *Proc. 22nd Int. Coastal Engrg. Conf.*, ASCE, 82-94.

## Acknowledgement

This efforts was supported by the Army Research Office under Contract No. DAAL03-92-G-0016.